OXFORD
SOT | Society of Toxicology
www.toxsci.oxfordjournals.org

TOXICOLOGICAL SCIENCES, 142(1), 2014, 56–73

doi: 10.1093/toxsci/kfu153
Advance Access Publication Date: July 30, 2014

Profiling Dose-Dependent Activation of p53-Mediated Signaling Pathways by Chemicals with Distinct Mechanisms of DNA Damage

Rebecca A. Clewell*,[1], Bin Sun*, Yeyejide Adeleye†, Paul Carmichael†, Alina Efremenko*, Patrick D. McMullen*, Salil Pendse*, O. J. Trask*, Andy White†, and Melvin E. Andersen*

*The Hamner Institutes for Health Sciences, Research Triangle Park, North Carolina 27709 and †Unilever, Safety and Environmental Assurance Centre, Colworth Science Park, Sharnbrook, Bedfordshire, MK44 1LQ, UK

[1]To whom correspondence should be addressed at Institute for Chemical Safety Sciences, The Hamner Institutes for Health Sciences, 6 Davis Drive, Research Triangle Park, NC 27709. Fax: (919) 558-1300. E-mail: rclewell@thehamner.org.

ABSTRACT

As part of a larger effort to provide proof-of-concept *in vitro*-only risk assessments, we have developed a suite of high-throughput assays for key readouts in the p53 DNA damage response toxicity pathway: double-strand break DNA damage (p-H2AX), permanent chromosomal damage (micronuclei), p53 activation, p53 transcriptional activity, and cell fate (cell cycle arrest, apoptosis, micronuclei). Dose-response studies were performed with these protein and cell fate assays, together with whole genome transcriptomics, for three prototype chemicals: etoposide, quercetin, and methyl methanesulfonate. Data were collected in a human cell line expressing wild-type p53 (HT1080) and results were confirmed in a second p53 competent cell line (HCT 116). At chemical concentrations causing similar increases in p53 protein expression, p53-mediated protein expression and cellular processes showed substantial chemical-specific differences. These chemical-specific differences in the p53 transcriptional response appear to be determined by augmentation of the p53 response by co-regulators. More importantly, dose-response data for each of the chemicals indicate that the p53 transcriptional response does not prevent micronuclei induction at low concentrations. In fact, the no observed effect levels and benchmark doses for micronuclei induction were less than or equal to those for p53-mediated gene transcription regardless of the test chemical, indicating that p53's post-translational responses may be more important than transcriptional activation in the response to low dose DNA damage. This effort demonstrates the process of defining key assays required for a pathway-based, *in vitro*-only risk assessment, using the p53-mediated DNA damage response pathway as a prototype.

Key words: toxicity pathways; p53; DNA damage response; dose-response; animal alternatives; three Rs

In 2007, the National Research Council (NRC) of the National Academy of Sciences released a report, "Toxicity Testing in the 21st Century: A Vision and a Strategy (TT21C)" (NRC, 2007), which called for a reorientation of toxicity testing. This approach focuses on evaluating the responses of toxicity pathways (i.e., normal cellular signaling pathways that can be perturbed by chemical exposures) in well-designed assays using human cells. Several related efforts are underway to evaluate the utility of *in vitro* assays for risk assessment, the majority of which focus on repurposing currently available assays as screening tools

(Collins *et al.*, 2008; Kavlock *et al.*, 2012). These efforts aim to reduce animal testing, increase the number of chemicals for which toxicity data are available, and reduce costs of chemical risk assessment by prescreening compounds with high-throughput assays and prioritizing high activity compounds for further testing in animals. By and large, these efforts still require animal testing for risk assessments. In contrast, the NRC recommended elimination of animal testing based on the clear evidence that high dose animal testing does not provide the necessary information for predicting human response to low dose chemical exposure.

Our goal is to develop *in vitro*-only risk assessments for several prototype toxicity pathways. The process requires the development of "fit-for-purpose" *in vitro* assays to examine cellular pathway responses (Andersen *et al.*, 2011; Boekelheide and Andersen, 2010). These assays should give multiple readouts that span modulatory, homeostatic, and adverse responses and provide data that can be used to create computational systems biology pathway models (Zhang *et al.*, 2010). These computational models would provide mechanistic understanding of the shape of dose-response curves, support low dose extrapolation from *in vitro* test results (Bhattacharya *et al.*, 2011), and predict regions of safety for human exposure without resorting to in-life animal assays.

The first step in this process is identification and development of appropriate *in vitro* assays for a specific toxicity pathway. This paper describes the first steps in defining the key readouts for the p53-mediated DNA damage response pathway and the development and implementation of several assays with prototype DNA damaging chemicals. Initial studies were performed in a human fibrosarcoma cell line (HT1080) expressing wild-type p53, and a second p53 competent human cell line (HCT 116) was used to confirm the HT1080 results. Three chemicals that induce different types of DNA damage were used to probe the cellular response: etoposide, methyl methanesulfonate, and quercetin. Etoposide is a topoisomerase II inhibitor, which forms a complex with DNA and topo II and prevents religation of double-strand breaks (Burden and Osheroff, 1998). Methyl methanesulfonate is an alkylating agent that methylates DNA bases (primarily adenine and guanine). Misrepair of these methylated bases leads to single-strand breaks and double-strand breaks (Ma *et al.*, 2011; Nikolova *et al.*, 2010; Wyatt and Pittman, 2006). Quercetin is a flavonoid that has been shown to act as an anti-oxidant at low doses and a pro-oxidant at higher doses (Min and Ebeler, 2008). Quercetin is able to cause DNA damage through formation of oxidative adducts, which leads to single- and double-strand breaks through misrepair, and has also been shown to act as a topoisomerase II inhibitor at higher doses (Cantero *et al.*, 2006).

Our goal was to start from first principles to demonstrate the process of defining key assays required for a pathway-based, *in vitro*-only risk assessment, using the p53-mediated DNA damage response pathway as the prototype. Although p53-independent processes can also affect cell fate (Bouska and Eischen, 2009; Yu and Zhang, 2009), this manuscript focuses on the p53-mediated DNA damage response. p53 is vital to prevention of fixed mutation and carcinogenicity (Hollstein *et al.*, 1991). p53 protein is activated in response to DNA damage through post-translational modification (phosphorylation). Initial activation of p53 appears to be determined by the type of DNA damage (single- and double-strand breaks, oxidative damage, etc.) and the activating protein kinases. Activated p53 functions as a recruitment factor for nuclear DNA repair enzymes and as a transcription factor (Fig. 1). It transcriptionally regulates key DNA damage response proteins that induce cell cycle arrest, DNA repair, and apoptosis in mammalian cells (Arias-Lopez *et al.*, 2006; Barak *et al.*, 1993;

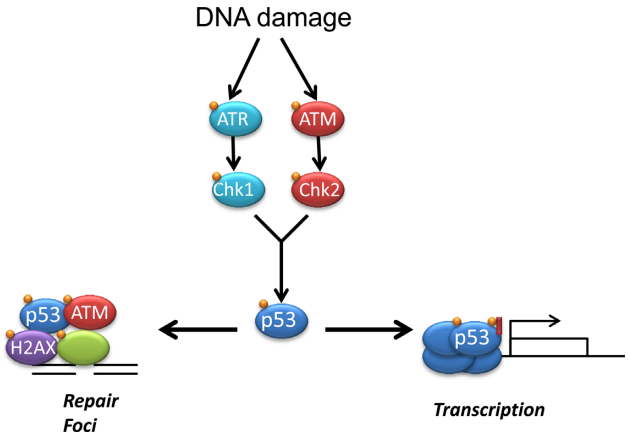

FIG. 1. Post-translational and transcriptional activities of p53 in response to DNA damage. ATM: ataxia telangiectasia mutated kinase. ATR: ataxia telangiectasia and Rad3-related protein kinase. Chk1: Chek 1 kinase. Chk2: Chek 2 kinase. pH2AX: phosphorylated histone 2AX. The unnamed oval represents repair proteins that are recruited to the sites of DNA damage. The specific repair proteins that are recruited are dependent upon the type of DNA damage. The small circle indicates phosphorylation, which leads to protein activation.

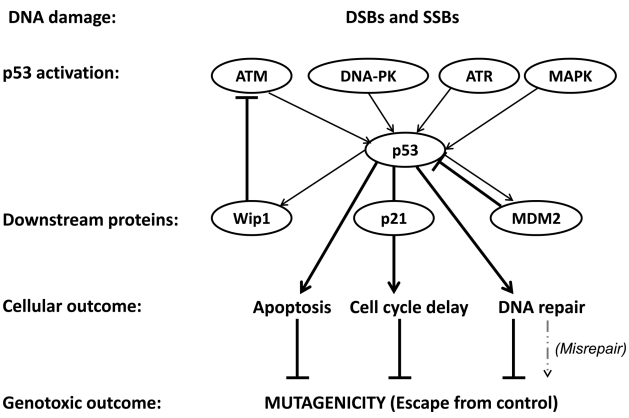

FIG. 2. Key elements in p53-mediated DNA damage response. Figure adapted from Loewer *et al.* (2010). ATM: ataxia telangiectasia mutated kinase. ATR: ataxia telangiectasia and Rad3-related protein kinase. DNA-PK: DNA-dependent protein kinase. MAPK: mitogen-activated protein kinases. Wip1: wild-type p53-induced phosphatase. MDM2: mouse double minute protein 2 homolog.

Chen and Sadowski, 2005; El-Deiry *et al.*, 1993; Harper *et al.*, 1993; Miyashita and Reed, 1995; Oda and Arakawa, 2000; Thornborrow *et al.*, 2002).

Although the response of p53 to DNA damage is multifactorial and involves many proteins, the key regulators have been described based on studies with ultraviolet (UV) and gamma irradiation (Batchelor *et al.*, 2011; Lahav *et al.*, 2004; Loewer *et al.*, 2010; Purvis *et al.*, 2012). Based on this understanding of the p53 pathway, we identified five main assay endpoints: DNA damage, p53 activation, p53 mediator proteins, cellular outcome, and permanent mutation, i.e., genotoxic outcome (Fig. 2). Assays were developed for each endpoint and response was measured over a wide of range of concentrations for the prototype chemicals. The resulting dose-response data were used to (1) map the p53 response network for each chemical and (2) evaluate the dose-response curves for each of the measured biomarkers. The purpose of collecting the in-depth dose-response data was to assess the conditions under which cellular response may prevent a net increase in heritable muta-

tion (adaptive response) and conditions at which perturbations of DNA structure are expected to propagate into fixed mutations in the genome and provide altered cells with the potential for autonomous growth (adverse outcome). Identifying this transition from the condition where DNA-repair processes can control any induced damage to one where there are sufficiently large degrees of damage leading to mutations is a key step in assessing adversity at the cellular level for DNA-reactive compounds (Boekelheide and Andersen, 2010).

MATERIALS AND METHODS

Reagents and antibodies. Etoposide (≥98%) (CAS no. 33419-42-0; Cat no. 152003; Lot no. 2249K) and quercetin (97%) (quercetin dehydrate; CAS no. 6151-25-3; Cat no. E7657; Lot no. 23925401) were purchased from LKT Laboratories and MP Biomedicals, respectively. Methyl methanesulfonate (99%) (CAS no. 66-27-3; Cat no. 129925; Lot no. 87569LJ) was purchased from Sigma-Aldrich (St. Louis, MO). Mouse anti-p53 (DO-1) (Cat no. sc-126; Lot no. G112) and glyceraldehyde 3-phosphate dehydrogenase (GAPDH) (0441; Cat no. sc-47724; Lot no. K1512) monoclonal antibodies were purchased from Santa Cruz Biotechnology (Santa Cruz, CA). Mouse anti-p-H2AX (Ser129) (3F2) (Cat no. MA1-2022; Lot no. MK160859) monoclonal antibody was from Pierce (Rockford, IL). Rabbit anti-p-H2AX (Ser129) (20E3) (Cat no. MA1-2022; Lot no. MK160859), p-p53 (ser15) (Cat no. 9718; Lot no. 8) and p-p53 (ser46) (Cat no. 2512; Lot no. 5) antibodies and Alexafluor 488-conjugated rabbit cleaved caspase 3 (Cat no. 9669; Lot no. 9) antibody were purchased from Cell Signaling Technology (Danvers, MA). Rabbit anti-p-p53 (ser15) (Cat no. 700439; Lot no. 1098699A) and Alexafluor 647-conjugated mouse anti-bromodeoxyuridine (BrdU) antibodies (Mo-BU1; Cat no. 35140; Lot no. 1113546) were obtained from Invitrogen (Carlsbad, CA). Horseradish peroxidase-conjugated anti-mouse (Cat no. W4021; Lot no. 0000038165) and anti-rabbit IgG (Cat no. W4011; Lot no. 0000038165) were obtained from Promega (Madison, WI). All other fluorochrome-conjugated secondary antibodies were obtained from Invitrogen.

Cell culture. HT1080 cells were purchased from the American Type Culture Collection (ATCC). The cells were grown under the conditions recommended by ATCC: Eagle's Minimum Essential medium (ATCC (Manassas, VA)) supplemented with 10% (v/v) heat-inactivated fetal bovine serum (FBS; Atlanta Biologicals, Flowery Branch, GA), 100-mg/l streptomycin, and 100 U/ml of penicillin G (Invitrogen) at 37°C in a humidified atmosphere of 95% air and 5% CO_2. HT1080 cells used in all experiments were passage number 30 or lower. The doubling time was approximately 16 h under these conditions. Cells were grown in 12-well plates for immunoblot analysis, 24-well plates for gene array studies, and 96-well plates for high-throughput flow cytometry or high content imaging studies.

Chemical treatment. Cells were plated in complete medium containing 10% heat-inactivated FBS and allowed to attach overnight. Stock solutions of chemicals were prepared in dimethyl sulfonate (DMSO) at 1000-fold higher concentrations than the final target doses. Stock solutions were aliquoted and stored at −20°C for up to 1 week. Dosing solutions were prepared immediately prior to treatment of the cells by diluting stock solutions 1:200 in complete media. Twenty four hours after seeding the cells, the medium in each well was supplemented with the dosing solutions (1:5 v/v), for a final chemical dilution of 1:1000 (0.1% vehicle). Cells were maintained in original complete medium throughout the course of the experiment. Immediately following treatment, medium was removed and the cells were washed with phosphate buffered saline (PBS) and prepared for subsequent analyses.

Adenosine triphosphate viability analysis. Cell viability was assessed using intracellular adenosine triphosphate (ATP) content after 4, 24, and 48 h of chemical treatment with 1, 3, 10, 30, or 100-μM etoposide; 1, 3, 10, 30, or 100-μM quercetin; or 1, 10, 100, 1000, or 10,000-μM methyl methanesulfonate. Viability studies were performed with three biological replicates, each with three technical replicates. Relative ATP content was measured using the ATPlite 1-Step Assay (ATPLite 1-Step; PerkinElmer Life Sciences, Boston, MA) according to the manufacturer's directions. As a quality control measure, viability was also measured as part of the high content imaging micronucleus assay (permeability dye) and the apoptosis assay (live/dead staining). The permeability dye and live/dead cell stain were included to ensure that the apoptosis and micronucleus results were not confounded by dying cells. These results were also used as additional measures of viability in addition to the ATP assay.

Immunoblot analysis. Cells were seeded at 200,000 cells/well in 12-well plates. 24 h after plating, cells were exposed to 1-μM etoposide, 30-μM quercetin, or 200-μM methyl methanesulfonate for 3, 8, or 24 h. After chemical treatment, cells were washed twice with PBS, homogenized in immunoblot buffer (0.1-M Tris-HCl pH8.0; 0.05-M ethylenediaminetetraacetic acid, pH 8.0; 0.5 M NaCl; 1% sodium dodecyl sulfate (SDS) and 1% sarkosyl) plus 1% protease inhibitor cocktail and 1% phosphatase inhibitor cocktail (Pierce). Protein levels were determined using a bicinchoninic acid assay kit (Pierce) according to manufacturer's instructions. Twenty micrograms of total protein was mixed with SDS-sample buffer (Invitrogen), heated to 90°C for 3 min, separated under reducing conditions on precast 4%–20% Tris-HCl gels (Invitrogen), and transferred to a nitrocellulose membrane. Nonspecific binding was blocked by incubating the membranes with blocking buffer (2.5% casein; 0.15-M NaCl, 0.01-M Tris, and 0.02% Thimerosal pH 7.6) for 2 h. Membranes were incubated with primary antibodies overnight at 4°C followed by a 2-h incubation in the appropriate secondary antibody. GAPDH was used as an internal control to ensure equal loading. Bands were detected by enhanced chemiluminescence (Pierce). Western blot studies were performed with three biological replicates, each with one technical replicate.

Protein dose-response analysis. HT1080 cells were plated into 96-well plate at 16,000/well. After 24 h, cells were treated with DMSO (vehicle control), etoposide, methyl methanesulfonate, or quercetin for various treatment times. The concentration of DMSO was 0.1% in all samples. For the initial range finding studies (dose and time), cells were treated with etoposide (0.003, 0.01, 0.03, 0.1, 0.3, 0.6, 1, 3, or 10μM), quercetin (1, 3, 10, 20, 30, 60, 80, 100μM), or methyl methanesulfonate (3, 10, 30, 100, 150, 200, 300, or 450μM) for 1, 2, 4, 6, 8, 16, or 24 h. For subsequent dose-response studies, the duration of chemical treatment was kept at 24 h. Dose-response studies for p53, p-p53, and p-H2AX were performed at the following doses: etoposide (0.003, 0.006, 0.01, 0.02, 0.03, 0.06, 0.1, 0.2, 0.3, 0.6, 1, 2, 3, 6, and 10μM), quercetin (0.06, 0.1, 0.2, 0.3, 0.6, 0.8, 1, 2, 3, 6, 8, 10, 20, 30, 60, 80, and 100μM), and methyl methanesulfonate (0.1, 0.2, 0.3, 0.6, 1, 2, 3, 6, 10, 20, 30, 60, 100, 125, 150, 175, and 200μM). Dose-response studies for mouse double minute 2 homolog (MDM2) protein, wild-type (wt) p53-induced phosphatase (Wip1), and p21 were performed at the

following doses: etoposide (0.003, 0.006, 0.01, 0.02, 0.03, 0.06, 0.1, 0.2, 0.3, 0.6, 1, 2, 3, 6, 10μM), quercetin (0.06, 0.1, 0.2, 0.3, 0.6, 0.8, 1, 2, 3, 6, 9, 10, 20, 30, 60,40, 80, and 100μM), and methyl methanesulfonate (0.1, 0.3, 1, 2, 3, 6, 10, 20, 30, 60, 100, 125, 150, 175, and 200μM). Protein expression studies were performed with three biological replicates, each with three technical replicates. Statistical significance was determined using 1-way ANOVA, with Dunnett's post-test.

Immediately after treatment, cells were trypsinized, transferred to 96-well v-bottom plates, and fixed with 4% formaldehyde, followed by incubation of 90% methanol on ice for 30 min. Methanol was removed and plate was washed with PBS once. Cells were permeabilized with 0.1% triton x-100 for 10 min and blocked with incubation buffer (0.5% BSA in 0.1% Triton X-100) for an additional 15 min. The plates were then incubated with appropriate primary antibodies diluted in incubation buffer at 4°C overnight, washed and incubated with secondary antibodies and/or fluorescent-conjugated primary antibodies plus Hoechst 33342. Plates were washed twice with PBS and analyzed on the BD Canto II flow cytometer (Becton Dickinson, Franklin Lakes, NJ). The following excitation (Ex) lasers and emission (EM) filters were used: p-p53 AF488 (Ex 488; Dichroic 502 LP; EM 530/30 (FITC channel)) and p53 AF647 (Ex 633; Dichroic none; EM 670LP (APC Channel)) or p-H2AX AF647 (633; Dichroic none; EM 670LP (APC Channel)). Data were collected and presented as fold increase compared with control.

Cell cycle analysis. HT1080 cells were plated into a 96-well plate at 16,000/well. After 24 h, cells were treated with DMSO (vehicle control), etoposide, methyl methanesulfonate, or quercetin. Chemical concentrations were as follows: etoposide (0.003, 0.006, 0.01, 0.02, 0.03, 0.06, 0.1, 0.2, 0.3, 0.6, 1, 2, 3, 6, 10μM), quercetin (0.06, 0.1, 0.2, 0.3, 0.6, 0.8, 1, 2, 3, 6, 9, 10, 20, 30, 60,40, 80, 100μM), and methyl methanesulfonate (0.1, 0.3, 1, 3, 6, 10, 20, 30, 60, 100, 125, 150, 175, 200μM). After exposure to appropriate chemicals for 22.5 h, cells were treated with 100-μg/ml BrdU for 1.5 h. Cells were harvested and transferred to 96-well v-bottom plates. After fixation with formaldehyde and methanol, cells were permeabilized with 0.1% Triton X-100/0.1 M HCl for 1 min on ice. The plates were centrifuged, supernatant was removed, and cells were washed once with DNA incubation buffer (0.15-mM NaCl and 15-mM trisodium citrate dehydrate). Cells were heated to 95°C for 5 min to denature DNA. Cells were then cooled on ice, centrifuged and denatured buffer was discarded. Cells were incubated over night with blocking buffer. Cells were then washed and incubated at room temperature for 1 h with Hoechst 33342 and AF-647-conjugated rabbit anti-BrdU antibody (1:100). The following excitation (Ex) lasers and emission (EM) filters were used: Hoechst (Ex 407; Dichroic Mirror none; EM 450/50 (Pacific Blue channel)); BrdU AF647 (Ex 633; Dichroic none; EM 670LP (APC Channel)). Cell cycle studies were performed with three biological replicates, each with three technical replicates. Statistical significance was determined using 1-way ANOVA, with Dunnett's post-test.

Multiplex analysis of apoptosis, necrosis, and p-p53 (ser46). Twenty four hours after plating, cells were treated with DMSO (vehicle control), etoposide, methyl methanesulfonate, or quercetin. Chemical concentrations were as follows: etoposide (0.0003, 0.001, 0.003, 0.006, 0.01, 0.02, 0.03, 0.1, 0.3, 0.6, 0.8, 2, 6, 10μM), quercetin (0.06, 0.1, 0.2, 0.3, 0.6, 0.8, 1, 2, 3, 6, 9, 10, 20, 30, 40, 60, 80, 100μM), and methyl methanesulfonate (0.1, 0.3, 1, 2, 3, 6, 10, 20, 30, 60, 100, 125, 150, 175, 200, 300, 450, 600μM). After 24-h chemical treatment, cells were incubated with aqua live/dead cell dye (Invitrogen) on ice for 30 min and washed once using PBS. Cells were then fixed with 4% formaldehyde and 90% methanol, followed by permeabilization and blocking. Plates were subsequently incubated with rabbit anti p-p53 (ser46) primary antibodies diluted in incubation buffer at 4°C overnight, followed by incubation of AF647-conjugated secondary antibodies for 1 h. Cells were washed once, blocked one more time with incubation buffer, and then incubated with AF488-conjugated rabbit anti-cleaved caspase 3 primary antibodies for another hour. Cells were washed twice with PBS and analyzed using flow cytometry. The following excitation (Ex) lasers and emission (EM) filters were used: Aqua live/dead dye (Ex 407; Dichroic Mirror none; EM 520/50—Amcyan channel); cleaved caspase3 AF488 (Ex 488; Dichroic 502 LP; EM 530/30 (FITC channel)); p-p53 (ser46) AF647 (Ex 633; Dichroic none; EM 670LP—APC Channel). The data were collected and presented as percent of entire population. Cell death studies were performed with three biological replicates, each with three technical replicates. Statistical significance was determined using 1-way ANOVA with Dunnett's post-test.

Micronucleus frequency and cell viability using high content imaging. HT1080 cells were seeded at a density of 3000 cells/well in optically clear collagen coated 96-well plates in complete medium and allowed to attach overnight before starting chemical treatment. Chemical concentrations were as follows: etoposide (0.0003, 0.0006, 0.001, 0.002, 0.003, 0.006, 0.01, 0.02, 0.03, 0.06, 0.1, 0.2, 0.3, 0.6, 1, 1.5, 2, 3μM), quercetin (0.06, 0.1, 0.2, 0.3, 0.6, 0.8, 1, 2, 3, 6, 9, 10, 20, 30, 40, 60, 80, 100μM), and methyl methanesulfonate (0.1, 0.3, 1, 3, 6, 10, 20, 30, 60, 100, 125, 150, 175, 200μM). Duration of chemical treatment was 1.5 doubling times (27 h). Cell staining was performed using the Cellomics Micronucleus Kit (Cat no. K1100011, Cellomics, Pittsburgh PA). Cellular dye solution was prepared according to the kit instructions and added to the cells. After 1-h incubation, the medium was removed, cells were washed once with complete medium, 100-μl complete medium containing DMSO (0.1%) or the test chemical was added to each well and cells were allowed to incubate for 27 h. Medium was then removed, cells were washed once with complete medium followed by addition of cytokinesis blocking buffer according to the Cellomics protocol, and cells were allowed to incubate overnight. Cells were prepared for bioimaging according to the Cellomics micronucleus protocol using three dyes to label the (1) nucleus and (2) cytoplasm, and (3) measure cytotoxicity (cell permeability). Fifty microliters of the Permeability Dye solution was added to each well and plate was incubated at 37°C for 30 min. Medium was then aspirated, cells were rinsed once with 100-μl complete media, and 100 μl of Fixation/Hoechst Dye solution was added to all wells. Plates were allowed to incubate at room temperature. After 20 min, Fixation/Hoechst Dye solution was aspirated, cells were rinsed twice with 100 μl of 1X Wash Buffer/well, and 200 μl of 1X Wash Buffer was added to each well. The plate was sealed, covered with aluminum foil, and stored at 4°C until bioimaging (less than 48 h).

Plates were scanned using a Cellomics ArrayScan VTI capturing 49 fields/well. Images were generated using a 20X/0.4NA objective and light-emitting diode (LED) excitation light source. All images were analyzed with the Cellomics micronucleus algorithm for identifying binucleated cells and micronuclei. The Cellomics 3-channel micronucleus algorithm has been well validated and optimized for analysis. Images were analyzed for percentage of micronucleus frequency in all binucleated cells. Scoring of micronuclei was performed using the Cellomics proprietary Micronucleus BioApplication software. Inclusion of the cy-

tokinesis blocker cytochalasin B ensures that cells are unable to complete daughter cell division following mitosis, allowing recent micronucleus events to be distinguished from previous events. Micronuclei were scanned in binucleated cells in which both nuclei were of similar size and intensity. Micronuclei were counted when their size was between 1/16 and 1/3 the size of the nuclei. Micronucleus frequency was expressed as % of binucleated cells with micronuclei. Dose-response curves for micronuclei were evaluated using the Lutz and Lutz hockey stick model (Lutz and Lutz, 2009) as described in the publication. Micronuclei studies were performed with three biological replicates, each with three technical replicates. Statistical significance was determined using 1-way ANOVA, with Dunnett's post-test.

Confirmation of HT1080 results with a second cell line. Limited protein dose-response studies were performed in a second cell line (HCT 116) to confirm the trends observed in the HT1080 cells (see Supplementary Data). HCT 116 cells are a human colorectal cell line expressing wild-type p53. HCT 116 cells were obtained from ATCC and cultured in Macoy's 5A medium supplemented with 10% (v/v) heat-inactivated FBS, 100-μg/l streptomycin, and 100-U/ml of penicillin G at 37°C in a humidified atmosphere of 95% air and 5% CO_2. The passages of HCT 116 cells were no more than 40 during all experiments. Cells were grown in 12-well plates for immunoblot analysis and 96-well plates for high-throughput flow cytometry studies. For flow cytometry dose-response studies of p-H2AX, phospho and total p53 and micronuclei, cells were exposed to etoposide (0.01, 0.03, 0.1, 0.3, 1.0, 3.0, 10, 20, 30, 60μM), quercetin (0.3, 1.0, 3.0, 10, 20, 30, 40, 60, 80, 100μM), or methyl methanesulfonate (0.3, 1.0, 3.0, 10, 30, 100, 200, 300, 450μM) for 24 h. Collection of cells, staining and flow cytometric and statistical analyses of protein levels were performed as described previously for HT1080 cells. For Western blots, HCT 116 cells were exposed to 1-μM etoposide, 30-μM quercetin, or 200-μM methyl methanesulfonate for 24 h. Immunoblot analyses were performed as described previously for the HT1080 cells. GAPDH was used as an internal control to ensure equal loading. All results represent three independent experiments for both HT1080 and HCT 116 cells.

Statistical analysis of proteins and cell fate assays. Statistical significance calculations were performed using a 1-way ANOVA and Dunnett's post-test in Prism 5.04 (GraphPad, La Jolla, CA). The lowest observed effect level (LOEL) is defined as the lowest concentration causing a statistically significant ($p \leq 0.05$) change in the measured parameter. LOELs for all dose-response studies (with the exception of the preliminary range-finding studies) are given in Table 1. The no observed effect level (NOEL) is defined as the test concentration immediately preceding the LOEL. For each of the dose-response studies (ATP viability, flow cytometric analyses of proteins, cell cycle, and apoptosis, as well as flow cytometric and high content analyses of micronucleus frequency and live/dead cell staining), results represent three independent biological replicates that were performed as separate experiments. Each biological replicate also consisted of three technical (in plate) replicates.

Benchmark dose analysis of protein expression and cell fate data. Bench Mark Dose (BMD) analysis on protein data were performed using United States Environmental Protection Agencies Benchmark Dose Software. The software used the concentration, mean response, standard deviation, and number of samples to calculate the Hill, exponential, and power models for the data. A constant variance, no restrictions on the parameters, and a benchmark response of 1 standard deviation difference from control were applied. BMD lower 95% confidence limits (BMDLs) were also calculated from the continuous linear models fit to the data. The other models available were not applicable. The BMD and BMDL (95% lower confidence interval for BMD) were chosen using the best *p*-values calculated for the models by the United States Environmental Protection Agencies Benchmark Dose Software.

Gene array studies, RNA isolation, and microarray hybridization. Gene array studies were performed with six biological replicates, each with one technical replicate. Statistical analyses are described below. HT1080 cells were grown in 24-well plates. Cells were treated with vehicle (0.1% DMSO), etoposide (0.003, 0.01, 0.03, 0.1, 0.3, 1.0, 3.0μM), quercetin (1, 3, 10, 30, 60, 80, 100μM), or methyl methanesulfonate (1, 3, 10, 30, 100, 300, 500μM) for 24 h. Immediately following treatment, total RNA was collected from the treated cells using the Qiaxtractor and the Qiagen VX reagent pack according to the manufacturer's protocol (Qiagen, Valencia, CA). A DNase 1 incubation was performed on all samples to remove any possible contamination of the RNA samples with cellular DNA (Qiagen). RNA samples were prepared for microarray hybridization using the GeneAtlas 3′ IVT Express Kit according to manufacturer's protocol (Applied Biosystems, Carlsbad, CA). Briefly, total RNA was reverse transcribed to synthesize first-strand cDNA. The cDNA was then converted into a double-stranded DNA template for transcription. Amplified cRNA (aRNA) was transcribed *in vitro*, with incorporation of a biotin-conjugated nucleotide. The aRNA was then purified to remove unincorporated NTPs, salts, enzymes, and inorganic phosphate, and samples were fragmented to prepare the biotin-labeled aRNA samples for hybridization onto Affymetrix GeneChip. Samples were loaded onto an HT HG-U133+ PM GeneChip array plate and run on the GeneTitan according to manufacturer's protocol (Applied Biosystems). The GeneChip HT HG-U133+ PM array plate utilizes the same content as the GeneChip Human Genome U133 Plus 2.0 Array cartridge, analyzes the relative expression level of more than 47,000 transcripts and variants, including more than 38,500 well-characterized genes and UniGenes, provides whole-genome coverage of the transcribed human genome on a single array in a 96-array configuration, and includes more than 54,000 probe sets and 1.3 million distinct oligonucleotide features. All gene array data discussed in this publication have been deposited in NCBI's Gene Expression Omnibus (Edgar *et al.*, 2002) and are accessible through GEO Series accession number GSE59368.

Statistical analysis of microarrays. Gene array analyses were performed based on data from six independent experiments (six biological replicates). Initial analysis of gene expression data was performed using Partek software (Partek Inc., St. Louis, MO). Arrays were robust multi-array average normalized (Irizarry *et al.*, 2003) and a 1-way ANOVA with interactions was performed to compare gene expression between the treated and control cells. Probability values were adjusted for multiple comparisons using a false discovery rate of 5%.

Benchmark dose analysis of microarray data. Benchmark doses were calculated with BMDExpress rel. 1.41 (Yang *et al.*, 2007). The four different models used to fit the data were power (power function restricted to $>= 1$), linear, 2° polynomial, and 3° polynomial. A constant variance, no restrictions on the parameters and a benchmark response of 1 standard deviation difference from control were applied. Benchmark dose lower 95% confi-

dence limits (BMDLs) were also calculated from the continuous linear models fit to the data. Only probes with a benchmark dose less than the maximum experimental concentration and with a model fit-*p*Value > 0.1 were retained for further analyses. Redundant probes matching the same gene were averaged to obtain a single gene-based benchmark dose value. After benchmark dose analysis a defined category analysis was performed, using Entrez Gene identifiers matched to their corresponding GeneGo pathway map ontology elements. Benchmark doses were only considered if the pathway had at least three elements (genes) with a benchmark dose (i.e., at least three genes each with benchmark dose < max. concentration and fit-*p*Value > 0.1).

Comparison of chemical-specific pathway activation from microarray data. A database of genes directly regulated by p53 was compiled from several published studies that examined p53 DNA binding sites using chromatin immunoprecipitation followed by high throughput DNA sequencing (ChIP-seq) in human cells after induction of DNA damage (Aksoy *et al.*, 2012; Cawley *et al.*, 2004; Kapranov *et al.*, 2002; Smeenk *et al.*, 2011). ChIP-seq data were available from cells in normal growth conditions and following treatment with chemical agents that induce different types of DNA damage (actinomycin D, etoposide, nutlin3a, 5-fluorouracil, and RITA). The Galaxy/Cistrome genome tool (Liu *et al.*, 2011) was used to map each bound interval to its nearest downstream gene within 10,000 bp from the start of interval. This gene list was then used to identify genes from our transcriptomic experiments that are directly regulated by p53 (genes directly or indirectly bound by p53). The p53-regulated genes that were differentially expressed with etoposide, quercetin, and methyl methanesulfonate treatment were then mapped to Gene Ontology (GO; Ashburner *et al.*, 2000) and Reactome (Vastrik *et al.*, 2007) pathways to uncover their roles in the response to DNA damage. Enrichment was determined using a hypergeometric test.

Comparison of chemical-specific pathway activation from protein and cell fate data. A "p53-normalized concentration" was established based on a similar level of p53 activation (approximately 25% of cells responding for total p53 at 24 h). This level of induction in p53 expression represents approximately half of the maximal induction observed with any of the three prototype chemicals. The resulting concentrations for comparison were 0.3-μM etoposide (27% responders), 30-μM quercetin (29% responders), and 200-μM methyl methanesulfonate (25% responders). For each measured endpoint (p-p53 (s15), p-H2AX, S-phase, M-Phase, etc.), the percent of maximal response was calculated for each chemical by dividing the response at each chemical concentration by the maximal response induced by any of the chemicals. For example, the largest response observed for p-p53 (s15) was at 10-μM etoposide (79% of the cells responding)—this was set as the maximal response level for p-p53 (s15). To determine the % of maximal response for all other concentrations of etoposide, as well as all concentrations of quercetin and methyl methanesulfonate, the response at each measured concentration was divided by 79 and multiplied by 100. The data points were then divided into quintiles: 0–20%, 21–40%, 41–60%, 61-80%, and 81–100% of maximal response. As p-ATM and p-ATR were not measured with flow cytometry, a qualitative estimate of relative induction of these kinases was inferred from visualization of the Western blots. This approach was also used to compare chemicals at a "p-H2AX normalized concentration" (approximately 35% of the cells responding for p-H2AX induction at 24 h) (see Supplementary Data).

RESULTS

Cell Viability

Cell viability was examined by measuring intracellular ATP (luminescence assay) over a wide range of concentrations for etoposide (1–100μM), quercetin (1–100μM), and methyl methanesulfonate (1μM–10mM) at 4, 24, and 48 h (Figs. 3A–C) to determine optimal experimental conditions. Minimal change was observed at 4 h. At 24 and 48 h, all chemicals showed >50% reduction in viability at the highest tested concentrations. Etoposide was toxic even at low concentrations (1μM) at 48 h (Fig. 3A). Viability was also measured using a permeability dye when performing micronucleus assay (0.0003–3-μM etoposide, 0.06–100-μM quercetin, and 0.1–200-μM methyl methanesulfonate) and using a live/dead cell stain when performing the apoptosis assay (0.0003–30-μM etoposide, 0.06–100-μM quercetin, and 0.1–600-μM methyl methanesulfonate). Results were highly similar between the three viability assays (see Figs. 3 and 8; Supplementary fig. 1). These results were used to set upper limits for test duration (24 h) and concentrations of etoposide (10μM), quercetin (100μM), and methyl methanesulfonate (450μM) based on 50% survival.

Time-Dependence of DNA Damage and Cellular Response

To determine the time point producing the most robust dose response, a variety of proteins associated with DNA damage response were analyzed by Western blot at 3, 8, and 24 h after treatment with relatively high concentrations (~50% viability at 24 h) of etoposide (1μM), quercetin (30μM), and methyl methanesulfonate (100μM) (Fig. 4). Protein markers for DNA damage (the histone protein p-H2AX), DNA damage-associated kinase activation (p-ATM (s1981), p-Chk2 (Thr68), p-ATR (s428)), activation of p53 (ac-p53 (k382), p-p53 (s15) and total p53), and downstream p53 transcriptional response (MDM2, p21) covered various components of the DNA damage response signaling pathway. It was not expected that all changes would occur within the same time frame. However, the goal was to identify a single time point which would best represent the trends in activation of the various proteins to facilitate multiplexing of dose-response assays.

There were notable differences in the protein response to the three chemicals, both in terms of the nature of the response and in their time courses (Fig. 4). Despite similar levels of p53, etoposide showed a much more rapid upregulation of p-ATM, p-H2AX, and p-p53. Further, the p53 transcriptional products MDM2 and p21 were differentially regulated by the three chemicals. Only etoposide caused a strong increase in p21. Etoposide and methyl methanesulfonate, but not quercetin, showed a strong upregulation of MDM2. Importantly, the 24-h time point encompassed all relevant protein changes (i.e., all of the proteins that were induced at early time points were still increased at 24 h) for each of the three chemicals. Even phosphorylation events (kinases, p-p53), which are expected to occur rapidly, showed greater induction at the later time points. Although it is clear that no one time point will be optimal for screening every relevant protein response to DNA damage, these data indicated that 24 h was the most suitable time point for screening for p53 pathway activation using these particular protein biomarkers.

More detailed analysis of the time course for p-p53, p53, and p-H2AX further supports the use of the 24-h time point for initial dose-response studies. Biomarkers for DNA damage (p-H2AX) and p53 activation (p-p53 and p53) were measured using flow cytometry at several time points following exposure to a range of concentrations of etoposide, quercetin, or methyl methanesulfonate. Data for p-p53 are shown in Figure 5A–C. Data for p-H2AX

TABLE 1. Comparison of activating concentrations across measured biomarkers*

	LOEL[a]			NOEL[b]			BMD[c]			BMDL[d]		
	ETP	QUE	MMS	ETP	QUE	MMS	ETP	QUE	MMS	ETP	QUE	MMS
p-H2AX	0.2	20	60	0.1	10	30	0.07	13	87	0.05	9	80
p-p53 (s15)	0.06	20	60	0.03	10	30	0.05	15	66	0.04	11	54
p53	0.2	30	100	0.1	20	60	0.09	13	94	0.06	9	81
WIP1	0.2	30	175	0.1	20	150	0.1	20	111	0.08	14	91
MDM2	0.06	20	100	0.03	10	60	0.04	13	44	0.03	8	31
p21	0.2	30	100	0.1	20	60	0.09	10	63	0.05	7	50
Cell Cycle[e]	0.2	20	125	0.1	10	100	0.06	10	78	0.05	6	61
Apoptosis[f]	0.6	60	600	0.3	40	300	0.2	49	361	0.2	44	237
p-p53 (s46)	0.6	40	150	0.3	30	125	0.3	29	74	0.2	21	51
Micronucleus	0.06	10	60	0.03	8	30	0.03	3	22	0.03	1	19
Gene Transcription	0.03[g]	10[g]	30[g]	0.01	3	10	0.2[h]	12[h]	118[h]	0.1[h]	8[h]	25[h]

*ETP = etoposide, QUE = quercetin, MMS = methyl methanesulfonate. All values in the table are expressed in terms of nominal media concentration (μM).
[a]Lowest observed effect level (μM) determined by first concentration with statistical significance ($p < 0.05$, 1-way ANOVA with Dunnett's post-test).
[b]No observed effect level (μM) determined by test concentration immediately preceding the LOEL.
[c]Benchmark dose (BMD) calculated based on a benchmark response of 1 standard deviation difference from control.
[d]BMD lower 95% confidence limit (BMDL).
[e]Values shown for the phase of the cell cycle that changed at the lowest concentrations of etoposide (G2/M), methyl methanesulfonate (G2/M), and quercetin (G1, S).
[f]Apoptosis measured using cleaved caspase 3 as a biomarker.
[g]Concentration (μM) with first observed statistically significant changes in expression of any individual gene.
[h]BMD (μM) and BMDL (μM) calculated based on significant enrichment of GeneGo pathway categories.

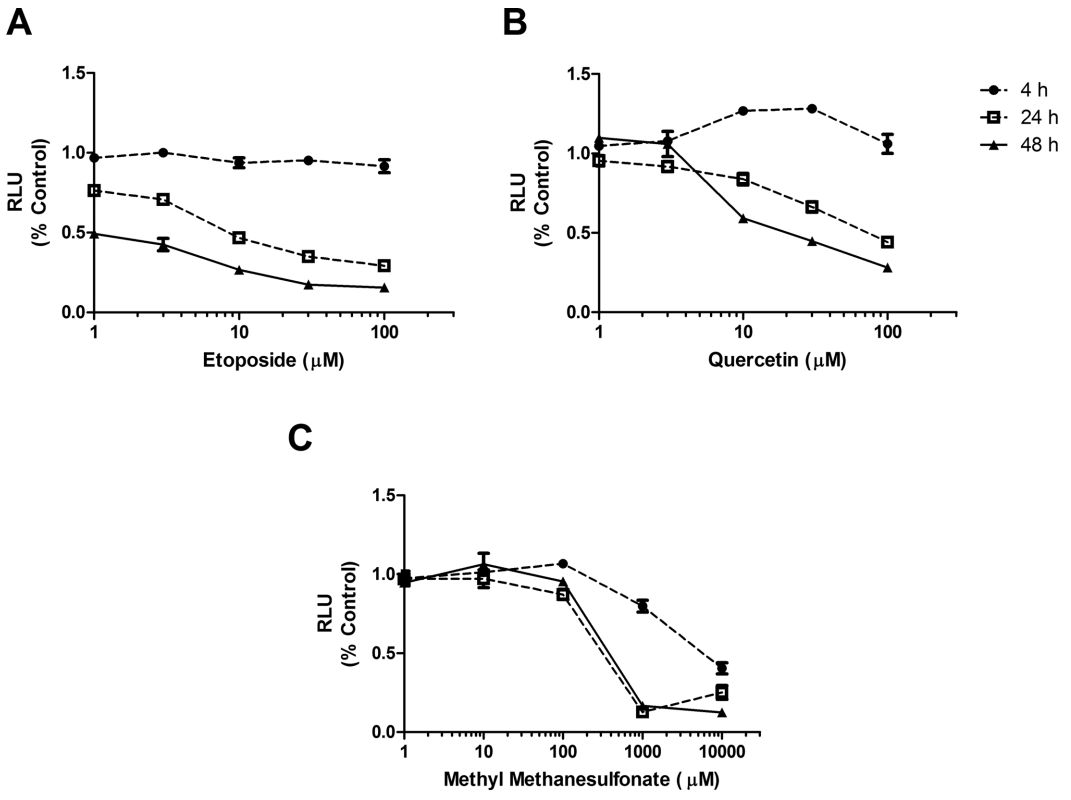

FIG. 3. Cell viability in HT1080 cells after treatment with (A) etoposide, (B) quercetin, or (C) methyl methanesulfonate. Cells were treated with DMSO, etoposide, quercetin, or methyl methanesulfonate for 4, 24, or 48 h. Cell viability was measured using an intracellular ATP content luminescence assay. The y-axes indicate the relative luminescence of the treated samples compared with control samples. Circles (4 h), squares (24 h), and triangles (48 h) represent the mean of three independent experiments (three biological and three technical replicates). Cross bars represent the standard error of the mean (SEM) of the data. RLU: relative fluorescence units. Etoposide caused a statistically significant ($p < 0.05$, 1-way ANOVA with Dunnett's post-test) decrease in viability with all concentrations at 24 and 48 h. No statistically significant changes were observed at 4-h etoposide exposure. Methyl methanesulfonate caused a significant ($p < 0.05$) decrease in viability with concentrations ≥1000μM at all time points. Quercetin caused a statistically significant increase in viability at 10 and 30μM at 4 h. At 24 and 48 h, quercetin caused a significant decrease in viability at concentrations ≥10μM.

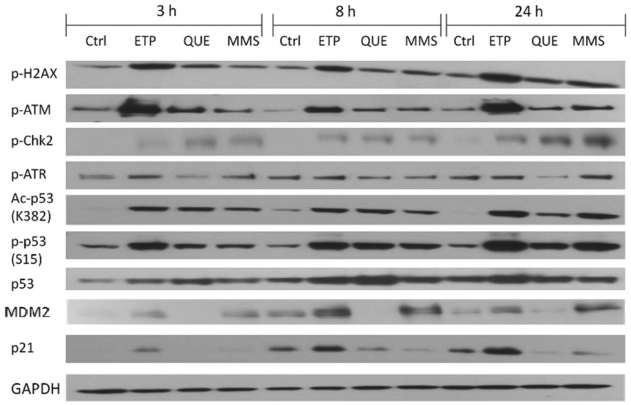

FIG. 4. Time course for DNA damage and p53 network response in HT1080 cells following exposure to etoposide, quercetin, or methyl methanesulfonate. Representative Western blots from three separate experiments are shown. HT1080 cells were exposed to 0.1% DMSO (control cells; Ctrl), 1-μM etoposide (ETP), 30-μM quercetin (QUE), or 200-μM methyl methanesulfonate (MMS) for 3, 8, or 24 h. Total cellular protein was isolated and subjected to immunoblot analysis. GAPDH was used as an internal control.

and total p53 are provided in the Supplementary Data (Supplementary fig. 2). Regardless of the chemical species, or the concentration used, p-H2AX, p53, and p-p53 were at maximal, or near maximal, levels at the 24-h time point.

Dose-Dependent Induction of Phosphorylated Histone Protein H2AX

In response to DNA damage, the histone protein H2AX is quickly phosphorylated at sites of double strand breaks, forming nuclear foci that can be imaged using p-H2AX-specific antibodies (Paull *et al.*, 2000). Measurement of p-H2AX serves as a marker of double-strand break DNA damage (Sedelnikova *et al.*, 2002). Consistent with its mode of action, topo II inhibition, and failed religation of DNA in M phase (Burden and Osheroff, 1998), etoposide was more efficient at inducing double-strand breaks than either quercetin or methyl methanesulfonate (Fig. 6A). Interestingly, quercetin induced double-strand breaks at lower concentrations than methyl methanesulfonate.

Dose-Dependent Activation of the p53 Pathway

Total and serine 15 phospho-p53. Serine 15 is one of the first sites on p53 modified in response to DNA damage and phosphorylation of serine 15 is associated with nuclear accumulation of p53 (Dumaz and Meek, 1999; Shieh *et al.*, 1997). Total p53 protein and p-p53 (ser15) were measured as markers of p53 activation (Fig. 6B–C). At basal conditions, p53 activity is kept low by its interaction with MDM2. MDM2 binds p53, sequestering p53 in the cytosol and targeting it for degradation. Following DNA damage, various DNA kinases (ATM, ATR, Chk1/2, DNA-PK) modify the p53 protein through phosphorylation, causing dissociation of the MDM2-p53 complex and accumulation of p53 protein.

The dose-dependence for p53 activation was similar to induction of p-H2AX (Fig. 6B). In fact, the LOELs for p-H2AX, total p53 or p-p53 for a particular chemical were remarkably similar (Table 1). All three proteins were significantly increased ($p < 0.05$, 1-way ANOVA with Dunnett's post-test) in the range of 0.1–0.2μM for etoposide, 20–30μM for quercetin, and 100–125μM with methyl methanesulfonate (see Table 1). The shapes of the dose-response curves were also generally similar across the biomarkers for DNA damage and p53 activation (p-H2AX, p-p53(ser15), and p53) with methyl methanesulfonate and quercetin. However, the shapes of the dose-response curves

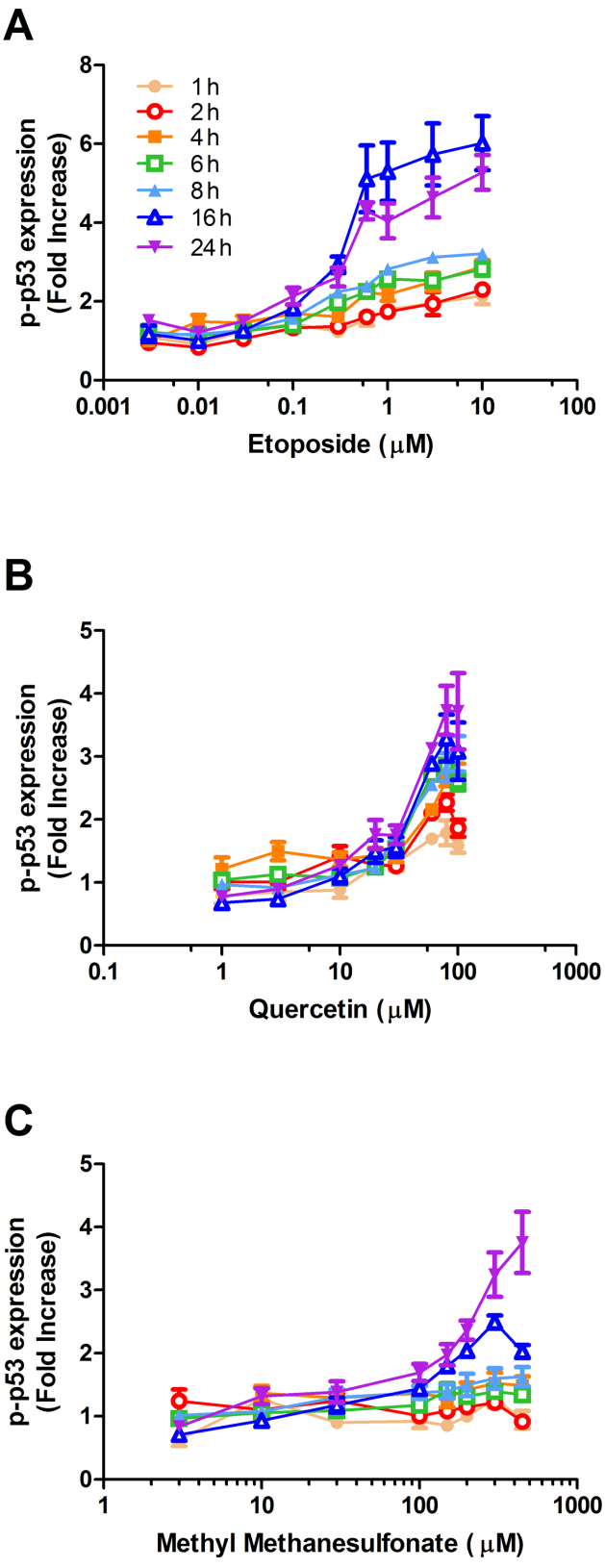

FIG. 5. Time- and concentration-dependent response for p-p53(ser15) induction in HT1080 cells following exposure to (A) etoposide, (B) quercetin, and (C) methyl methanesulfonate. Cells were treated with DMSO (0.1%), etoposide, quercetin, or methyl methanesulfonate for 1, 2, 4, 6, 8, 16, or 24 h and analyzed for p-p53 using flow cytometry. Circles and triangles represent the mean of three independent experiments (three biological replicates, each with three technical replicates). Bars represent the standard error of the mean (SEM).

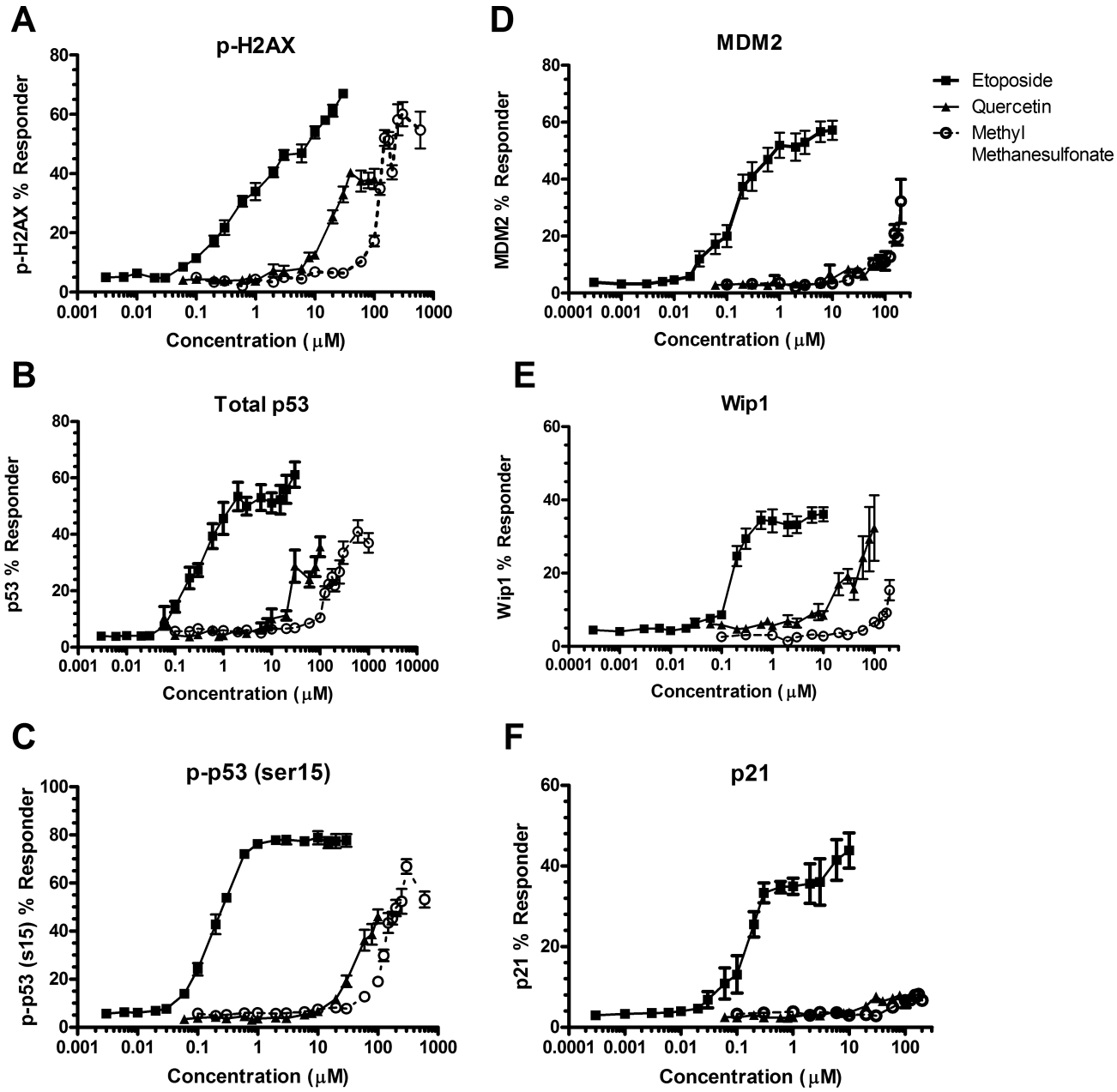

FIG. 6. Induction of (A) p-H2AX, (B) total p53, (C) p-p53(ser15), and (D–F) p53 effector proteins following 24-h etoposide, quercetin, and methyl methanesulfonate treatment. Circles, squares, and triangles represent the mean of three independent experiments (three biological replicates, each with three technical replicates). Cross bars represent the standard error of the mean (SEM). The lowest statistically significant ($p < 0.05$) concentrations are shown as LOELs in Table 1.

for p-H2AX and p-p53 were notably different with etoposide. Whereas the curve for p-H2AX was fairly linear across concentrations, the response for p-p53 and total p53 had plateaus at concentrations well below the highest tested concentration of etoposide. It is possible that quercetin and methyl methanesulfonate may also have exhibited a plateau in p53 response at higher doses than those tested. However, cytotoxicity prohibited testing at higher doses for these two chemicals.

These results were confirmed in a second cell line—the human colon carcinoma cell line HCT 116 (Supplementary fig. 3A). Although the HCT cells were generally less sensitive than the HT1080 cells, the dose-response trends were similar between the two cell lines. The shapes of the dose-response curves and LOELs were similar for the measured endpoints (p53, p-p53, and pH2AX) whether treated with etoposide, quercetin, or methyl methanesulfonate (data not shown). LOELs ranged from 1–3μM for etoposide (Supplementary fig. 3A). LOELs for p53, p-p53, and pH2AX were also similar for quercetin (20–40μM) (Supplementary fig. 3A). LOELs for methyl methanesulfonate ranged from 300–450μM (Supplementary fig. 3A). Although the two cell lines showed differing sensitivity to the chemicals, the consistency between the two p53-competent cell lines in terms of dose-response trends demonstrates that the trends observed in the HT1080 p53 response network are not specific to a single cell line.

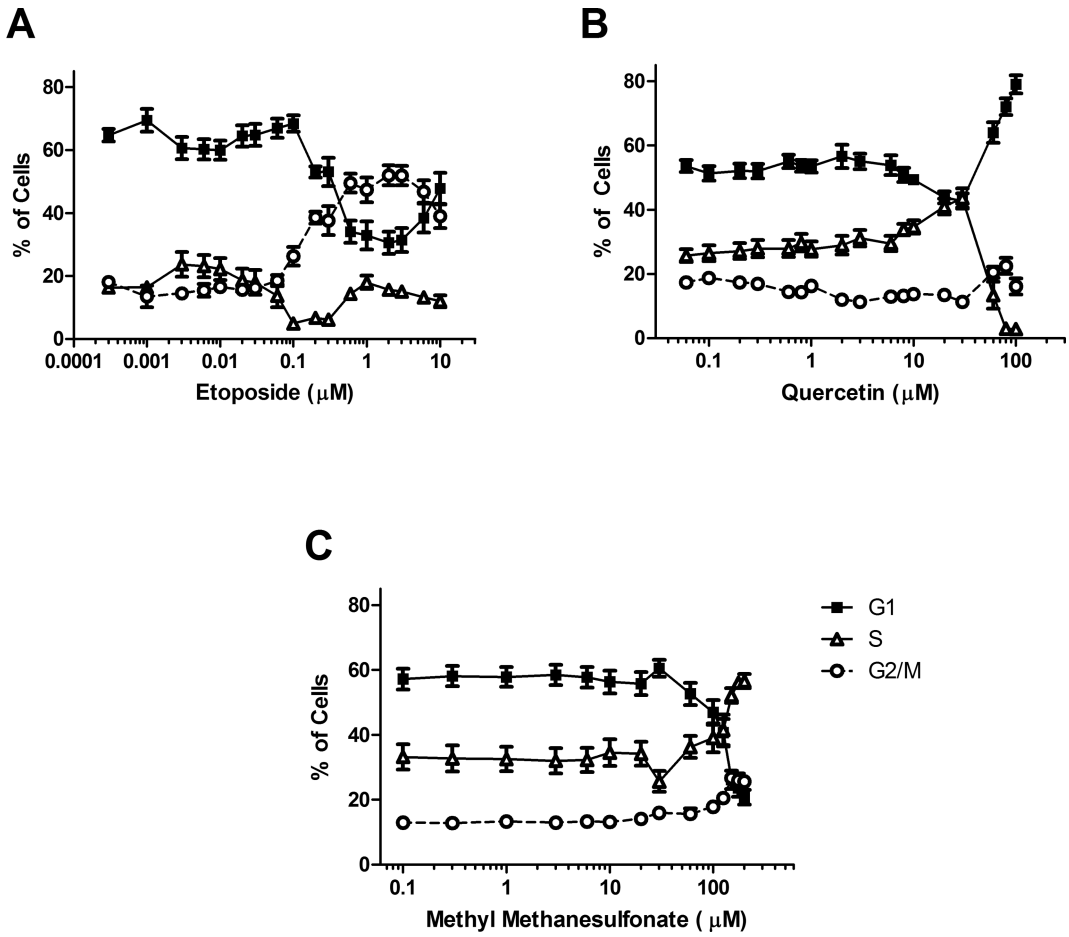

FIG. 7. Cell cycle effects following 24-h (A) etoposide, (B) quercetin, and (C) methyl methanesulfonate treatment. Circles, squares, and triangles represent the mean of three independent experiments (three biological replicates, each with three technical replicates). Cross bars represent the standard error of the mean (SEM). The lowest statistically significant ($p < 0.05$) concentrations are shown as LOELs in Table 1.

Upregulation of p53-mediated proteins. p21, Wip1, and MDM2 are direct transcriptional targets of p53. Wip1 and MDM2 are negative regulators of p53. Wip1 phosphatase inactivates ATM kinase leading to reduced phosphorylation of p53, whereas MDM2 interacts directly with p53 as described above. p21 is a major mediator protein for the p53 pathway, playing an important role in p53-mediated cell cycle arrest (G1/S transition). Based on initial immunoblot results (Fig. 4), the three prototype chemicals had distinctly different effects on p21, Wip1, and MDM2 expression. To verify the immunoblot results and quantitatively characterize the dose response for expression of these effector proteins, Wip1, MDM2, and p21 protein levels were measured in HT1080 cells across concentrations using flow cytometry following etoposide, quercetin, and methyl methanesulfonate exposure (24 h) (Fig. 6D–F). All three chemicals induced Wip1, and the Wip1 dose-response curves for each of the chemicals were similar to the dose response for p53 activation (Fig. 6E and Table 1). However, MDM2 and p21 clearly show chemical-specific differences. Although MDM2 is induced at concentrations of etoposide and methyl methanesulfonate where p53 is increased, quercetin has little effect on MDM2, even at concentrations that maximally activate p53 (100μM) (Fig. 6D). p21 only shows a strong upregulation with etoposide (Fig. 6F). The dose-response curves for p21 did not follow those of p53 or p-p53(ser15) for methyl methanesulfonate or quercetin. Thus, at chemical treatments causing similar levels of DNA damage (p-H2AX; Fig. 6A) and similar levels of p53 activation, the three chemicals produce different activation of p53 target genes. This differential activation of p21 and MDM2 was confirmed in HCT 116 cells (Supplementary fig. 3B).

Evaluation of Cell Fate

In response to DNA damage, p53 initiates several transcriptional programs designed to prevent heritable alterations in the DNA structure. When proliferating cells encounter DNA damage, p53 can initiate cell cycle arrest, in order to allow repair of DNA damage before continuing with cellular division. However, if DNA damage is too severe, p53 initiates programmed cell death (apoptosis). Markers of cellular fate (cell cycle arrest, apoptosis) were examined across concentrations of etoposide, methyl methanesulfonate, and quercetin in the HT1080 cells.

Cell cycle delay. Cell cycle was assessed by staining for DNA content and BrdU (S-phase) and analyzing the cells by flow cytometry (Fig. 7A–C). Etoposide caused an increase in the number of cells in G2/M, while decreasing S and G1 phase cells (Fig. 7A). In contrast to etoposide and methyl methanesulfonate, quercetin showed a biphasic dose response for cell cycle arrest (Fig. 7B). At concentrations >20μM, the number of cells in S-phase was moderately increased. However, higher quercetin concentra-

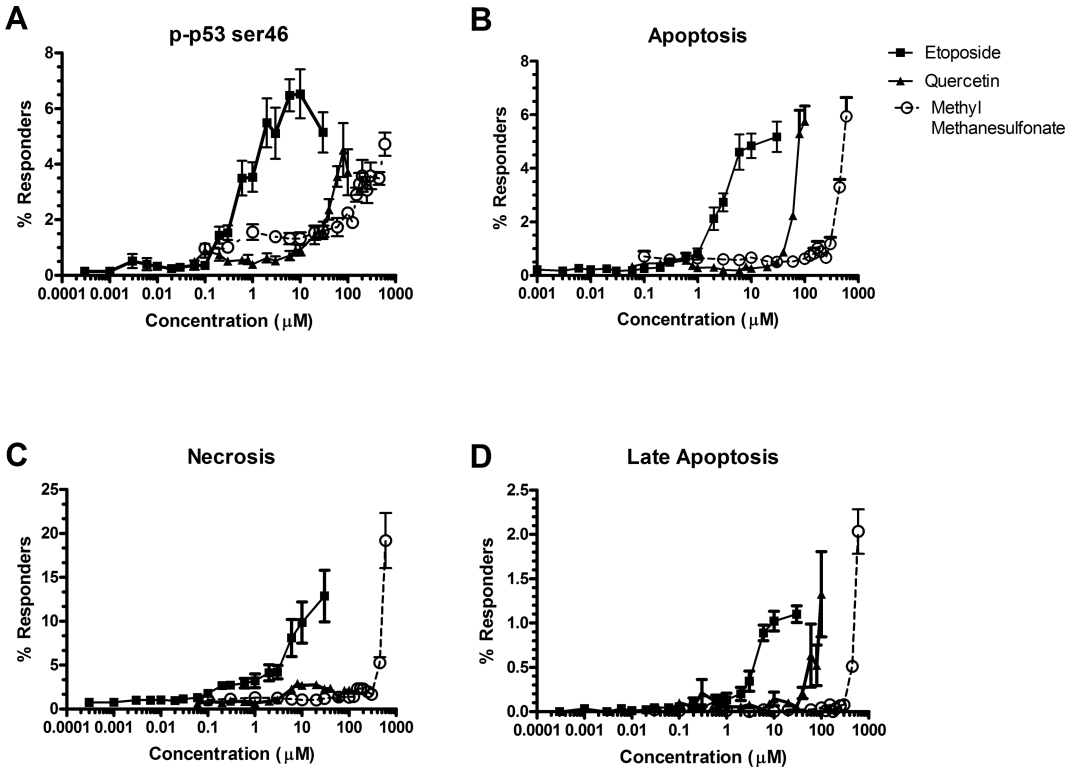

FIG. 8. Induction of (A) p-p53(ser46), (B) apoptosis, and (C) necrosis following 24-h etoposide, quercetin, and methyl methanesulfonate treatment. Circles, squares, and triangles represent the mean of three independent experiments (three biological replicates, each with three technical replicates). Cross bars represent the standard error of the mean (SEM). (B) Apoptosis indicates the percent of cells stained positive for cleaved caspase 3. (C) Necrosis indicates the percent of cells stained positive for membrane permeability dye. (D) Late apoptosis indicates percent of cells co-stained with cleaved caspase 3 and membrane permeability dye. The lowest statistically significant ($p < 0.05$) concentrations are shown as LOELs in Table 1.

tions (>60μM) decreased the number of cells in S phase and increased the number of cells in G1. Methyl methanesulfonate significantly increased the number of cells in M- and S-phase and decreased the number of cells in G1 at 100μM (Fig. 7C).

Apoptosis. Induction of apoptosis was assessed using simultaneous staining for cleaved caspase 3 and p-p53 (s46), a post-translational modification associated with p53-mediated apoptosis (D'Orazi *et al.*, 2002) (Fig. 8A–D). To verify that the measures of caspase activation were not affected by necrotic cells, a stain for increased membrane permeability (necrosis) was also included (Fig. 8C). Late apoptosis (Fig. 8D) is characterized by cells that stained positive for both necrosis (increased permeability) and cleaved caspase 3, whereas those cells designated as apoptotic (Fig. 8B) stained only for cleaved caspase 3. All three chemicals induced apoptosis at 24 h, with a similar maximal response (7–8% of cells) (Fig. 8B). Generally, p-p53 (ser 46) was induced at lower concentrations than cleaved caspase 3 (Fig. 8A and Table 1). Interestingly, the majority of etoposide-induced apoptotic cells were also p-p53 (s46) positive, whereas only a small portion of methyl methanesulfonate- or quercetin-induced apoptotic cells were co-stained with p-p53 (s46), indicating p53-independent pathways may be important for quercetin and methyl methanesulfonate-induced apoptosis.

Induction of Micronuclei

Micronuclei are formed when pieces of a chromosome or entire chromosomes are not incorporated into the daughter nuclei during mitosis (Samanta and Dey, 2012). Exposure to clastogenic DNA damaging compounds may induce micronucleus formation by increasing the number of unrepaired double-strand breaks, either through direct formation of double strand breaks, or by inducing DNA damage that is not faithfully repaired. Additionally, aneugenic chemicals may interfere with spindle formation and cell division leading to chromosome loss (aneuploidy). The micronucleus assay, which has been standardized under the OECD guidelines (OECD, 2010), is a widely used screening tool for genotoxic compounds. We used the micronucleus assay as a measure of permanent damage (i.e., any permanent (irreparable) alteration of the chromosome structure without designating whether micronuclei consisted of whole or partial chromosomes). The maximum micronucleus induction was much higher after etoposide treatment compared with methyl methanesulfonate or quercetin (Fig. 9A–C) in keeping with the much greater induction of double-strand break DNA damage (p-H2AX) and other markers of cellular response that indicate etoposide is more potent DNA damaging compound (Figs. 6–8). Although methyl methanesulfonate and quercetin induce different types of DNA damage (alkylation vs. oxidative damage), they both show a similar capacity for micronucleus induction, with a maximum fold change over controls of 4–5 (Fig. 9B and 9C). When the LOELs were compared across chemicals, etoposide was most potent followed by quercetin and methyl methanesulfonate (Table 1).

Many genotoxic chemicals appear to have nonlinear, or threshold, dose-response curves in genotoxicity (or mutation) assays (Bryce *et al.*, 2010; Calabrese *et al.*, 2011; Doak *et al.*, 2007; Elhajouji *et al.*, 2011; Platel *et al.*, 2011). The potential for threshold-like behavior in the micronuclei response curves was evaluated using a model that can test whether a threshold

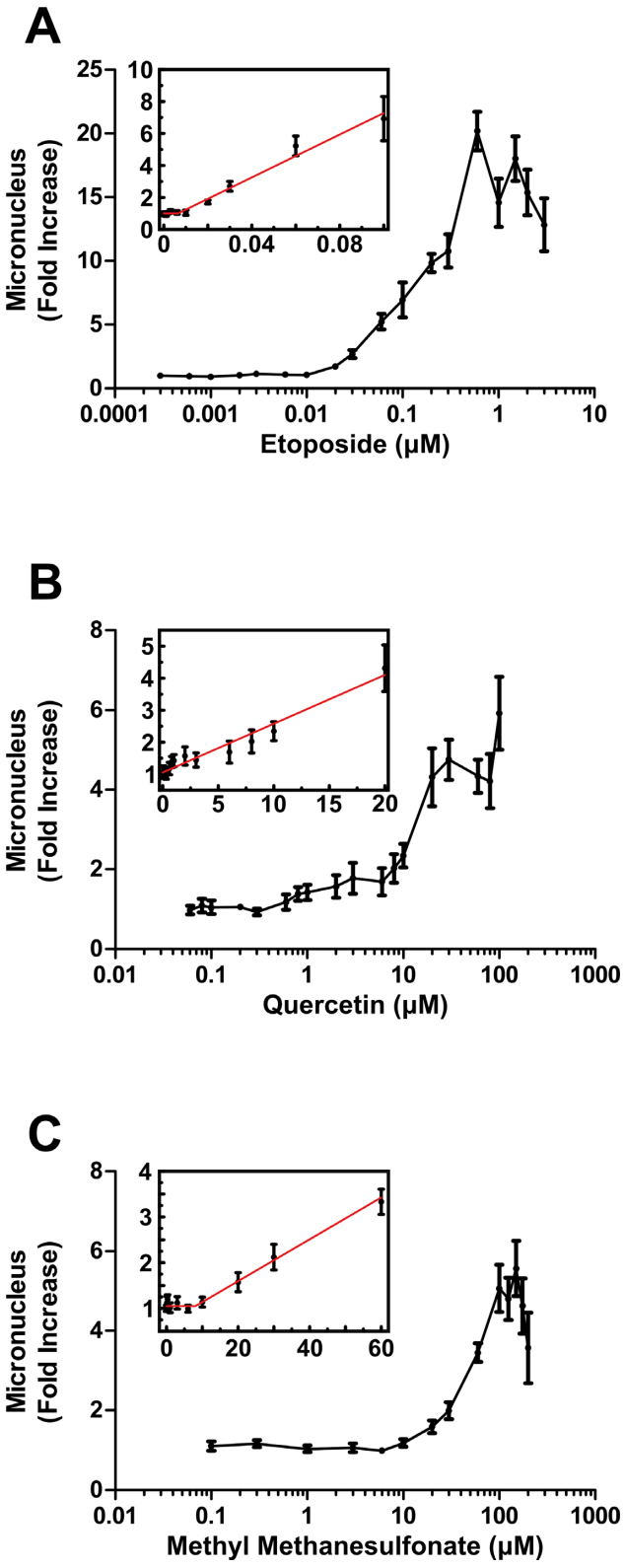

FIG. 9. Induction of micronuclei following (A) etoposide, (B) quercetin, and (C) methyl methanesulfonate treatment. Circles represent the mean of three independent experiments (three biological replicates, each with three technical replicates). Cross bars represent the standard error of the mean (SEM). Insets show data for concentrations near the transition point on a linear scale, together with the model predicted using the Lutz and Lutz hockey stick model (Lutz and Lutz, 2009). The Lutz model p-values for the micronucleus curves were 0.30, 0.99, and 0.048 for etoposide, quercetin, and methyl methanesulfonate, respectively. The lowest statistically significant ($p < 0.05$) concentrations are shown as LOELs in Table 1.

model is more likely than a linear model (Lutz and Lutz, 2009). Although this analysis does not "prove" threshold behavior, a p-value less than 0.05 supports the hypothesis that the dose-response curve is nonlinear and more likely to exhibit threshold behavior than a linear relationship. The Lutz model p-values for the micronucleus curves were 0.30, 0.99, and 0.048 for etoposide, quercetin, and methyl methanesulfonate, respectively. Thus, methyl methanesulfonate shows a statistically significant deviation from linear behavior, whereas etoposide and quercetin do not. The insets in Figure 9 show the micronuclei response at the transitional concentrations of etoposide, quercetin, and methyl methanesulfonate, together with the predicted Lutz and Lutz model.

Comparison of Dose-Response Across Protein and Cell Fate Endpoints

Relative sensitivities of the various biomarkers were analyzed in three ways: NOEL/LOEL, benchmark dose (BMD), and 95% lower confidence interval for the benchmark dose (BMDL). These values were then compared across protein and cell fate biomarkers for each individual chemical (Table 1). Despite the different levels of cellular regulation that were examined with in-depth dose-response studies, the majority of assays were activated at similar concentrations for a given chemical. For example, when p53 activation, double-strand break induction (p-H2AX), cell cycle, apoptosis, and micronucleus induction are compared for etoposide, the LOELs (first statistically significant change, $p \leq 0.05$) for all of the endpoints were within a very narrow concentration range (0.06–0.2μM), with the exception of cell death/apoptosis. The induction of apoptosis/necrosis occurred at higher concentrations (≥ 0.6μM). Similar trends were noted with methyl methanesulfonate and quercetin. Only apoptosis (cleaved caspase 3) showed a different concentration dependence than any of the other biomarkers. The trends for benchmark doses were similar; all biomarkers, with the exception of apoptosis/necrosis, had similar benchmark doses within an individual chemical. Notably, micronucleus induction was one of the most sensitive endpoints. Although several doses of each of the chemicals showed no increase in micronuclei, induction of micronuclei was observed at concentrations less than or equal to those required for a significant increase in activation of p53. This same trend was observed in HCT 116 cells when the LOELs were compared across the p-H2AX, p53, and p-p53(ser15) and micronucleus endpoints (see Supplementary table 1).

Evaluation of Transcriptomic Dose Response

In an effort to compare the dose response for gene transcription with induction of micronuclei, whole genome arrays were run for HT1080 cells treated with various concentrations of etoposide, methyl methanesulfonate, or quercetin. Concentrations were based on the micronuclei dose-response curve to represent regions of (1) no change from background, (2) transition from no change to induction of micronuclei, and (3) maximal induction of micronuclei. The lowest concentrations with statistically significant gene changes were 0.03-μM etoposide, 10-μM quercetin, and 30-μM methyl methanesulfonate, which corresponded to 14, 4, and 1 gene(s), respectively. In order to compare the dose response for transcriptional activation with the protein endpoints, the benchmark dose was calculated for each gene and the average BMD for each biological process GO category was determined (Yang *et al.*, 2007). The BMDs for the most sensitive pathway with each chemical are given in Table 1. Interestingly, the most sensitive pathways for the three chemicals were not related to DNA damage or p53 activation. The gene categories with the lowest BMDs were "immune response", "cytoskeleton re-

modeling", and "development" for etoposide, methyl methanesulfonate, and quercetin, respectively (Supplementary table 1). A more detailed list of BMDs and categories for the top pathways are in the Supplementary Data (Supplementary table 1). Whether the gene changes are compared based on LOEL or BMD for enriched GO categories, transcriptional activation occurred at concentrations within the range of those that induced micronucleus formation. Although the lowest doses did not induce micronuclei, there were significant increases in micronuclei at doses that did not affect p53 transcriptional response, indicating that p53 transcriptional response does not prevent induction of micronuclei.

Comparison of Protein and Cell Fate Response at Concentrations Causing Similar p53 Activation

Although the data show similar dose-response trends (BMDs/LOELs) for the various biomarkers within a single chemical, it is clear from the protein and cell fate data that the cellular response differs across the three prototype chemicals. Because the chemicals induced different types of DNA damage and have different potencies, however, the comparison across chemicals cannot be performed simply on the basis of chemical concentration. In an effort to standardize the concentrations of etoposide, methyl methanesulfonate, and quercetin, we established a "p53-normalized concentration" that induced a similar level of p53 activation (approximately 25% of cells responding for total p53 at 24 h) for each chemical. The resulting concentrations for comparison were 0.3-μM etoposide, 30-μM quercetin, and 200-μM methyl methanesulfonate (see the Materials and Methods section). This level of induction in p53 expression represents approximately half of the maximal induction observed with any of the three prototype chemicals (Fig. 6). By using these p53-normalized concentrations we could compare the p53 program across chemicals without the added complication of concentration/potency.

Figure 10 summarizes the protein and cell fate responses for each chemical at the p53-normalized concentration. Despite similar levels of induction of p53, the activated p53 response network varies significantly among the three chemicals. Etoposide induced a much stronger ATM response than did the other two chemicals, and a greater induction of Wip1 and MDM2 than did either quercetin or methyl methanesulfonate. Furthermore, only etoposide induced p21. Despite this strong activation of the p53 pathway, and the much stronger induction of apoptosis than either methyl methanesulfonate or quercetin, the response to etoposide was least successful at preventing permanent DNA damage (micronuclei). The same trends hold true when the responses were normalized by p-H2AX level (35% of the cells responding for p-H2AX) (Supplementary fig. 4).

In addition to the clear differences in downstream signaling, this figure highlights the chemical-specific activation of p53. Although all three chemicals show evidence of activation of p53 through ATM kinase, ATM plays a much larger role in etoposide response than in responses to methyl methanesulfonate or quercetin. Further, ATR kinase is not involved in quercetin response at all. The amino acid residue (serine 15) of p53 that is targeted by these kinases shows the same trend as the activated kinases: etoposide > methyl methanesulfonate > quercetin. The strong induction of total p53 without a corresponding response by ATM/ATR indicates that quercetin must activate p53 via another mechanism.

Comparison of Transcriptional Program at Concentrations Causing Similar p53 Activation

The protein and cell fate data indicate that the p53 pathway is differentially activated by the three prototype chemicals. The transcriptomic data collected at concentrations that induce similar levels of total p53 expression (0.3-μM etoposide, 200-μM methyl methanesulfonate, 30-μM quercetin) were evaluated to determine whether the chemicals induce different p53-dependent transcriptional programs (see Supplementary Data for differentially expressed genes—Supplementary table 1). We determined the portion of the transcriptional response directly regulated by p53 by combining our gene expression microarray data with published ChIP-seq data (see the Materials and Methods section). The resulting lists consisted of 103, 149, and 255 genes both differentially expressed and regulated directly by p53 for etoposide, quercetin, and methyl methanesulfonate, respectively (Supplementary table 1). Of these genes, 38 were common to all three chemicals, constituting a core DNA damage response that depends on p53 regulation irrespective of the nature of DNA damage. Etoposide, quercetin, and methyl methanesulfonate had 14, 50, and 147 uniquely regulated genes, respectively, indicating mechanism-specific p53 responses across chemicals (Fig. 11A).

The core DNA damage response and the genes unique to etoposide, methyl methanesulfonate, or quercetin were evaluated using the GO (Ashburner *et al.*, 2000) and Reactome (Matthews *et al.*, 2009) pathway databases to identify cellular processes associated with the differentially expressed genes. Due to the small number of differentially expressed genes, none of the pathways were significantly enriched using the Reactome database ($p < 10^{-2}$, hypergeometric test, Benjamini-Hochberg correction). However, the processes associated with the differentially expressed genes reveal trends that can provide insight into the p53 transcriptional response (see Supplementary table 1). The pathways associated with the genes that the three chemicals had in common were those expected for p53 regulation: apoptosis, nucleotide excision repair, and cell cycle checkpoints (see Supplementary table 1). Interestingly, the core p53-mediated response induced by all three chemicals was enriched in GO terms related to apoptosis and response to DNA damage (Fig. 11B), whereas the p53-mediated genes specific to a single chemical were not. This observation further indicates that these 38 core genes constitute a general p53-mediated DNA damage response program.

DISCUSSION

High-throughput assays were developed in a human cell line expressing wild-type p53 (HT1080) for several key readouts for the p53-mediated DNA damage response toxicity pathway. More limited data were collected in a second cell line (HCT 116). Although the HCT 116s were generally less sensitive to the chemicals, the trends observed in the p53 activation and the comparison of dose response for various endpoints were consistent between the HT1080 and HCT 116 cells, indicating that the conclusions drawn from the HT1080 studies are not specific to a particular cell line.

Dose-response data for three prototype compounds with different mechanisms of DNA damage allow important comparisons that can improve our understanding of the p53 toxicity pathway (Figs. 5–9). The data collected in this paper were used to map the p53 network for chemicals with different mechanisms of action at concentrations that cause a similar induction

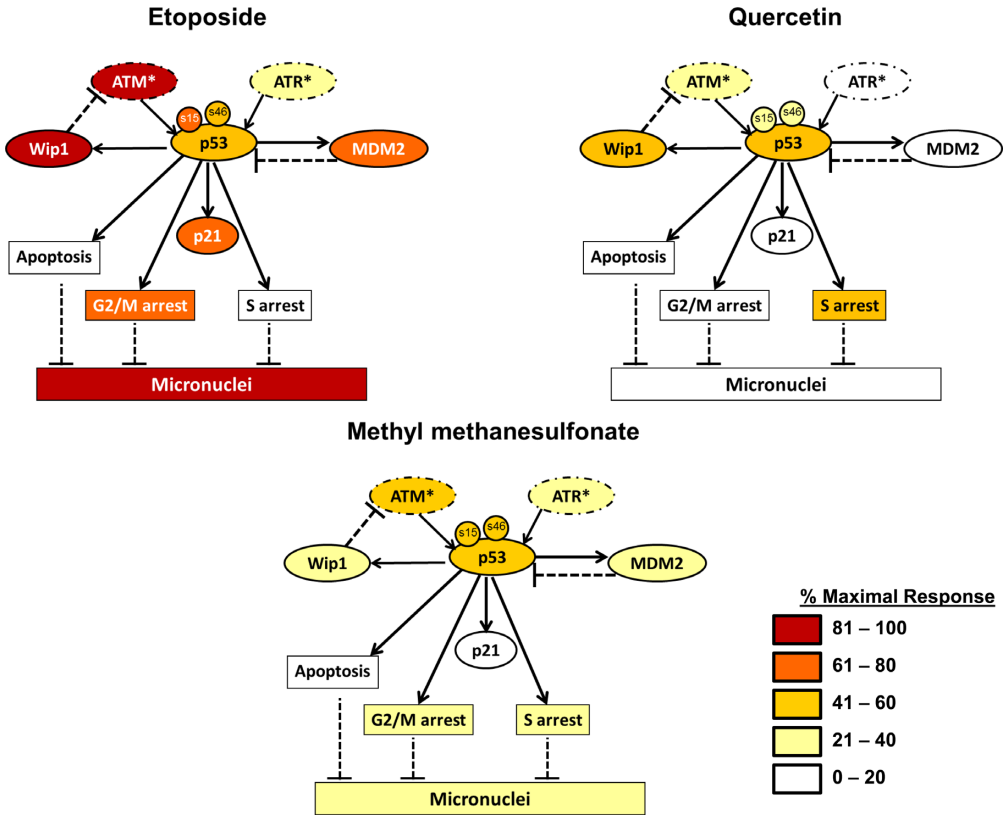

FIG. 10. Activation of protein and cell fate response at concentrations of etoposide, quercetin, or methyl methanesulfonate concentrations causing similar induction of p53. A p53-normalized concentration was established based on a similar level of p53 activation (approximately 25% of cells responding for total p53 at 24 h). This level of induction in p53 expression represents approximately half of the maximal induction observed with any of the three prototype chemicals. The resulting concentrations for comparison were 0.3-μM etoposide, 30-μM quercetin, and 200-μM methyl methanesulfonate. The degree of orange coloring indicates the degree of upregulation for a particular protein or process. For each endpoint, the percent of maximal response was calculated for each chemical. The response data were then divided into quintiles: 0–20%, 21–40%, 41–60%, 61–80%, and 81–100% of maximal response.

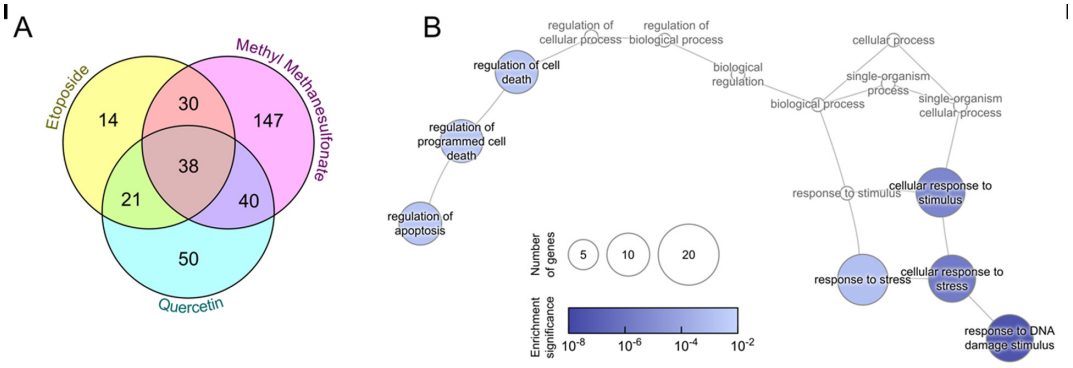

FIG. 11. Characterization of the damage mechanism-independent p53 response. (A) Venn diagram of genes differentially expressed genes regulated by p53 following exposure to etoposide, quercetin, or methyl methanesulfonate, which have been previously shown to be regulated by p53 binding. (B) Functional annotation graph of Gene Ontology (GO) terms enriched in the genes regulated by p53 and differentially expressed in response to exposure to all three chemicals. Terms are connected according to the structure of the parent-child relationships defined by GO. Blue terms are statistically enriched, relative to their prevalence in the genome ($p < 10^{-2}$, hypergeometric test, Benjamini-Hochberg correction). The size of node corresponds to the number of genes annotated with a given term.

of p53. These also provided an understanding of dose dependence of p53 response to different types of chemical-induced DNA damage. Evaluation of cellular response across chemicals and across concentrations led to two important conclusions: (1) the p53 transcriptional program is chemical specific and (2) the p53 transcriptional response does not prevent permanent DNA damage (micronuclei) induction at low concentrations.

The p53 Transcriptional Program is Chemical Specific

The p53 response appears to be determined by the type of chemical damage (i.e., single- vs. double-strand breaks). Studies with gamma and UV irradiation showed that UV irradiation, which primarily induces single-strand breaks through failed repair of thymidine dimers, activated the ATR kinase pathway (Brown and Baltimore, 2003). Alternatively, gamma irradiation, a strong

inducer of double-strand breaks, activates p53 through ATM kinase (Batchelor *et al.*, 2011). However, our studies show that p53 response to chemical-induced DNA damage cannot be classified simply by single- or double-strand breaks. In fact, when chemical response is compared at concentrations causing a similar upregulation of p53, the p53-dependent transcriptional program is markedly different across our three prototype compounds. Etoposide, which binds DNA and inhibits topo II religation of replicating DNA, activates a transcriptional program that leads to G2/M-phase arrest and apoptosis. Of the three chemicals, only etoposide showed an apoptotic response at concentrations that were not overtly cytotoxic. The pro-oxidant quercetin activates a program that favors G1/S arrest and DNA repair processes (evidenced by fewer micronuclei per double-strand break). Methyl methanesulfonate, an alkylating agent that causes single- and double-strand breaks through base excision repair and/or replication fork collapse (Ma *et al.*, 2011; Nikolova *et al.*, 2010), induces a program intermediate between that of etoposide and quercetin, with arrest in both G2/M and S phase and a modest apoptotic response at higher doses that also cause necrosis.

p53 activity is determined by the number and type of post-translational modifications and interaction with specific cofactors (Beckerman and Prives, 2010; Meek and Anderson, 2009; Murray-Zmijewski *et al.*, 2008; Xu, 2003). In particular, kinase activation is important for p53's release from MDM2, nuclear translocation, and transcriptional activation. Furthermore, post-translation modifications may modify p53 binding affinity for its response elements and, depending on the type and location of the modification, lead to different patterns of gene transcription (Beckerman and Prives, 2010; Smeenk *et al.*, 2011). Our study clearly demonstrates different patterns of kinase activity and post-translational modifications across the three chemicals. Etoposide had a much stronger induction of p-ATM than either quercetin or methyl methanesulfonate. p-ATR was transiently induced with methyl methanesulfonate and etoposide, but not quercetin. Serine 15 phospho-p53, which is a target of both ATR and ATM, also showed differences among the chemicals: Etoposide showed the greatest increase followed by methyl methanesulfonate and quercetin. Serine 46 phospho-p53 was much higher in etoposide and methyl methanesulfonate-treated cells than quercetin. The current study did not focus on upstream signaling of p53. However, these preliminary results indicate that the immediate cellular response and early activation of p53 is chemical specific and decisions about the p53 transcriptional response may, in fact, be made very early in the response pathways (i.e., prior to transcription). Other kinases, such as DNA-PK, the ATM/ATR-dependent kinases Chk2 and Chk1, and mitogen-activated kinases (MAPKs), are able to phosphorylate p53 at serine 15 and other amino acid residues (ser6, ser9, ser20, thr18, ser37, ser392, etc.). We are currently evaluating the early kinase response in more detail to identify the kinases involved in chemical-specific activation of the p53 pathway.

Evaluation of the p53 transcriptional program (differential expression of genes directly regulated by p53) revealed a set of core genes related to apoptosis and cell cycle arrest. However, etoposide, methyl methanesulfonate, and quercetin also initiated chemical-specific p53 activity. Thus, although there is a core network of p53 regulated genes, p53 also initiates additional transcriptional programs that lead to more specific chemical responses. Although our efforts to evaluate these chemical-specific networks did not yield statistically significant enrichment of GO or Reactome pathways, the Reactome database provided insight into the processes that may be uniquely activated by our three chemicals. For example, the top-ranked pathways (most highly enriched) associated with quercetin unique genes were related to interferon signaling, which is regulated by the transcription factor STAT1 (signal transducers and activators of transcription 1). STAT1 can form a complex with p53 and ATM, acting as a cofactor for p53 transcriptional regulation and enhancing p53-mediated apoptosis (Townsend *et al.*, 2004; Youlyouz-Marfak *et al.*, 2008). Top-ranked pathways associated with methyl methanesulfonate unique genes, however, were related to Notch signaling. The Notch pathway, which is associated with cellular differentiation, also has cross-talk with p53 via the mastermind-like (MAML) proteins. MAML proteins act as coactivators of Notch-mediated and p53-mediated transcriptional activation (Zhao *et al.*, 2007). MAML1 binding to p53 stabilizes the p53 proteins and enhances apoptotic response. The top-ranked pathways associated with etoposide (though admittedly there was only very small enrichment) were associated with MyD88, a protein implicated in toll-like receptor activation of NF-κB (nuclear factor kappa-light-chain-enhancer of activated B cells). NF-κB is a transcription factor that binds p53 and acts as co-regulator for gene transcription (Schneider *et al.*, 2010). Overall, our results indicate that a generic, protective transcriptional response to DNA damage—regardless of the initiating event—supports cell cycle arrest and apoptosis. Chemical-specific recruitment of co-regulators, which may enhance particular functions of p53, such as apoptosis or senescence, augments this generic response. Interaction with co-regulators may be mediated by post-translational modification of p53- or p53-independent activation of other pathways (NF-kB, STAT1, etc.) by different chemicals.

The p53 Transcriptional Response Does Not Prevent Micronucleus Induction at Low Concentrations

A quantitative understanding of the dose response underpins chemical risk assessment. In the effort to extrapolate high dose effects observed in laboratory experiments to low dose environmental exposures, it is necessary to describe the dose-response behavior of a chemical as accurately as possible. For chemicals with nonlinear response curves, estimating risk for low dose exposures from high dose data is particularly challenging. One of the more contentious conventions in risk assessment is the default assumption of low-dose linearity for genotoxicity, wherein genotoxic agents are considered to induce DNA-damage proportional to the administered dose. This dogma is based on the assumption that even a single molecule of a DNA reactive chemical may cause a mutation and thereby increase the risk for cancer. However, this assumption fails to consider nonlinearities resulting from biokinetic processes and cellular defense mechanisms. Some genotoxic chemicals exhibit threshold-like responses in mutation and genotoxicity assays both *in vivo* and *in vitro* (Bryce *et al.*, 2010; Gocke and Müller, 2009; Johnson *et al.*, 2009; Pottenger *et al.*, 2009). *In vivo* dosing often results in nonlinear serum and tissue kinetics due to complex biokinetic processes, including saturable uptake, metabolism, and clearance. *In vitro* kinetics can also be complex, as cellular dose is a product of several processes, including binding to proteins, binding to plastic, evaporation, and the interaction between the culture medium and the cells (Blaauboer, 2010). Further, studies with alkylating agents have provided strong evidence for repair as the mechanism by which threshold behavior for mutagenicity might be achieved (Doak *et al.*, 2007; Johnson *et al.*, 2009; Swenberg *et al.*, 1995; Thomas *et al.*, 2013).

Although it is not possible to "prove" threshold behavior statistically, it is possible to directly test the linearity of dose-response curves (Lutz and Lutz, 2009). Compounds that fail this

test are not likely follow the low-dose linearity model. Application of this statistical framework revealed that methyl methanesulfonate has a highly nonlinear response, whereas etoposide and quercetin are more consistent with a linear model. The hypothesis that DNA repair is able to prevent fixed mutation at low concentrations implies that activation of p53 and induction of protective responses (cell cycle arrest, repair protein transcription) would occur at lower concentrations than those required for micronucleus induction. When in-depth dose-response data were compared across endpoints, activation of the p53 transcriptional response did not occur at concentrations below those causing micronucleus formation. In fact, the micronucleus assay was one of the most sensitive endpoints for our three prototype chemicals. Thus, p53 transcriptional response cannot explain the observed threshold behavior with micronuclei for methyl methanesulfonate.

In addition to its transcriptional activity, p53 has a role in non-transcriptional DNA repair (Fig. 1). p53, together with several other scaffold proteins, kinases, and repair proteins, localizes at the sites of double-strand breaks and forms repair centers (Al Rashid *et al*., 2005). These repair centers are able to repair DNA damage prior to any transcriptional activities. Studies with gamma irradiation showed that repair center formation is more efficient at low doses (Neumaier *et al*., 2011), a phenomenon that may provide a mechanistic explanation for nonlinear mutagenicity response curves. Non-transcriptional activity of p53 is likely to be more important in repairing low dose, early DNA damage. Our ongoing work now focuses on the role of repair center formation in cellular response to low concentrations of genotoxic chemicals in order to define regions of safety for genotoxicity.

SUPPLEMENTARY DATA

Supplementary data are available online at http://toxsci.oxfordjournals.org/.

FUNDING

Unilever, PLC.

REFERENCES

Aksoy, O., Chicas, A., Zeng, T., Zhao, Z., McCurrach, M., Wang, X. and Lowe, S. W. (2012). The atypical E2F family member E2F7 couples the p53 and RB pathways during cellular senescence. *Genes Dev.* **26**, 1546–1557.

Andersen, M. E., Clewell, H. J., Carmichael, P. L. and Boekelheide, K., (2011). Can case study approaches speed implementation of the NRC report, "toxicity testing in the 21st century, a vision and a strategy"? *ALTEX* **28**, 175–182.

Arias-Lopez, C., Lazaro-Trueba, I., Kerr, P., Lord, C. J., Dexter, T., Iravani, M., Ashworth, A. and Silva, A. (2006). p53 modulates homologous recombination by transcriptional regulation of the RAD51 gene. *EMBO Rep.* **7**, 219–224.

Ashburner, M., Ball, C. A., Blake, J. A., Botstein, D., Butler, H., Cherry, J. M., Davis, A. P., Dolinski, K., Dwight, S. S., Eppig, J. T., *et al*. (2000). Gene ontology: Tool for the unification of biology. The Gene Ontology Consortium. *Nat. Genet.* **25**, 25–29.

Barak, Y., Juven, T., Haffner, R. and Oren, M., (1993). Mdm2 expression is induced by wild type p53 activity. *EMBO J.* **12**, 461–468.

Batchelor, E., Loewer, A., Mock, C. and Lahav, G. (2011). Stimulus-dependent dynamics of p53 in single cells. *Mol. Syst. Biol.* **7**, 488.

Beckerman, R. and Prives, C. (2010). Transcriptional regulation by p53. *Cold Spring Harb. Perspect. Biol.* **2**, a000935.

Bhattacharya, S., Zhang, Q., Carmichael, P. L., Boekelheide, K. and Andersen, M. E. (2011). Toxicity testing in the 21 century, defining new risk assessment approaches based on perturbation of intracellular toxicity pathways. *PLoS ONE* **6**, e20887.

Blaauboer, BJ. (2010). Biokinetic modeling and in vitro-in vivo extrapolations. *J. Toxicol. Environ. Health B Crit. Rev.* **13**, 242–252.

Boekelheide, K. and Andersen, M.E. (2010). A mechanistic redefinition of adverse effects—A key step in the toxicity testing paradigm shift. *ALTEX* **27**, 243–252.

Bouska, A. and Eischen, C. M. (2009). Mdm2 affects genome stability independent of p53. *Cancer Res.* **69**, 1697–1701.

Brown, E. J. and Baltimore, D. (2003). Essential and dispensable roles of ATR in cell cycle arrest and genome maintenance. *Genes Dev.* **17**, 615–628.

Bryce, S. M., Shi, J., Nicolette, J., Diehl, M., Sonders, P., Avlasevich, S., Raja, S., Bemis, J. C. and Dertinger, S. D. (2010). High content flow cytometric micronucleus scoring method is applicable to attachment cell lines. *Environ. Mol. Mutagen.* **51**, 260–266.

Burden, D. A. and Osheroff, N. (1998). Mechanism of action of eukaryotic topoisomerase II and drugs targeted to the enzyme. *Biochim. Biophys. Acta* **1400**, 139–154.

Calabrese, E. J., Stanek, E. J., III and Nascarella, M. A. (2011). Evidence for hormesis in mutagenicity dose-response relationships. *Mutat. Res.* **726**, 91–97.

Cantero, G., Campanella, C., Mateos, S. and Cortes, F. (2006). Topoisomerase II inhibition and high yield of endoreduplication induced by the flavonoids luteolin and quercetin. *Mutagenesis* **21**, 321–325.

Cawley, S., Bekiranov, S., Ng, H. H., Kapranov, P., Sekinger, E. A., Kampa, D., Piccolboni, A., Sementchenko, V., Cheng, J., Williams, A. J., *et al*. (2004). Unbiased mapping of transcription factor binding sites along human chromosomes 21 and 22 points to widespread regulation of noncoding RNAs. *Cell* **116**, 499–509.

Chen, J. and Sadowski, I. (2005). Identification of the mismatch repair genes PMS2 and MLH1 as p53 parget genes by using serial analysis of binding elements. *Proc. Natl Acad. Sci. U.S.A.* **102**, 4813–4818.

Collins, F. S., Gray, G. M. and Bucher, J. R. (2008). Toxicology. Transforming environmental health protection. *Science* **319**, 906–907.

Doak, S. H., Jenkins, G. J., Johnson, G. E., Quick, E., Parry, E. M. and Parry, J. M. (2007). Mechanistic influences for mutation induction curves after exposure to DNA-reactive carcinogens. *Cancer Res.* **67**, 3904–3911.

Dumaz, N. and Meek, D. W. (1999). Serine 15 phosphorylation stimulates p53 transactivation but does not directly influence interaction with HDM2. *EMBO J.* **18**, 7002–7010.

D'Orazi, G., Cecchinelli, B., Bruno, T., Manni, I., Higashimoto, Y., Saito, S., Gostissa, M., Coen, S., Marchetti, A. and Del Sal, G. (2002). Homeodomain- interacting protein kinase-2 phosphorylates p53 at Ser46 and mediates apoptosis. *Nat. Cell Biol.* **4**, 11–19.

Edgar, R., Domrachev, M. and Lash, A. E. (2002). Gene Expression Omnibus: NCBI gene expression and hybridization array data repository. *Nucleic Acids Res.* **30**, 207–210.

El-Deiry, W. S., Tokino, T., Velculescu, V. E., Levy, D. B., Parsons, R., Trent, J. M., Lin, D., Mercer, W. E., Kinzler, K. W. and Vogelstein, B. (1993). WAF1, a potential mediator of p53 tumor

suppression. *Cell* **75**, 817–825.
Elhajouji, A., Lukamowicz, M., Cammerer, Z. and Kirsch-Volders, M. (2011). Potential thresholds for genotoxic effects by micronucleus scoring. *Mutagenesis* **26**, 199–204.
Gocke, E. and Müller, L. (2009). *In vivo* studies in the mouse to define a threshold for the genotoxicity of EMS and ENU. *Mutat. Res.* **678**, 101–107.
Harper, J. W, Adami, G. R., Wei, N., Keyomarsi, K. and Elledge, S. J. (1993). The p21 Cdk-interacting protein Cip1 is a potent inhibitor of G1 cyclin-dependent kinases. *Cell* **75**, 805–816.
Hollstein, M., Sidransky, D., Vogelstein, B. and Harris, C. C. (1991). p53 mutations in human cancers. *Science* **253**, 49–53.
Irirzarry, R. A., Hobbs, B., Collin, F., Beazer-Barclay, Y. D., Antonellis, K. J., Scherf, U. and Speed, T. P. (2003) Exploration, normalization, and summaries of high density oligonucleotide array probe level data. *Biostatistics*, **4**, 249–262.
Johnson, G. E., Doak, S. H., Griffiths, S. M., Quick, E. L., Skibinski, D. O., Zaïr, Z. M. and Jenkins, G. J. (2009). Non-linear dose-response of DNA-reactive genotoxins: Recommendations for data analysis. *Mutat. Res.* **678**, 95–100.
Kapranov, P., Cawley, S. E., Drenkow, J., Bekiranov, S., Strausberg, R. L., Fodor, S. P. and Gingeras, T. R. (2002). Large scale transcriptional activity in chromosome 21 and 22. *Science* **296**, 916–919.
Kavlock, R., Chandler, K., Houck, K., Hunter, S., Judson, R., Kleinstreuer, N., Knudsen, T., Martin, M., Padilla, S., Reif, D., *et al.* (2012). Update on EPA's ToxCast program: Providing high throughput decision support tools for chemical risk management. *Chem. Res. Toxicol.* **25**, 1287–1302.
Lahav, G., Rosenfeld, N., Sigal, A., Geva-Zatorsky, N., Levine, A. J., Elowitz, M. B. and Alon, U. (2004) Dynamics of the p53-Mdm2 feedback loop in individual cells. *Nat. Genet.*, **36**, 147–150.
Liu, T., Ortiz, J. A., Taing, L., Meyer, C. A., Lee, B., Zhang, Y., Shin, H., Wong, S. S., Ma, J., Lei, Y., *et al.* (2011). Cistrome: An integrative platform for transcriptional regulation studies. *Genome Biol.* **12**, R83.
Loewer, A., Batchelor, E., Gaglia, G. and Lahav, G. (2010) Basal dynamics of p53 reveal transcriptionally attenuated pulses in cycling cells. *Cell*, **142**, 89–100.
Lutz, W. K. and Lutz, R. W. (2009). Statistical model to estimate a threshold dose and its confidence limits for the analysis of sublinear dose-response relationships, exemplified for mutagenicity data. *Mutat. Res.* **678**, 118–122.
Matthews, L., Gopinath, G., Gillespie, M., Caudy, M., Croft, D., de Bono, B., Garapati, P., Hemish, J., Hermjakob, H., Jassal, B., *et al.* (2009). Reactome knowledgebase of human biological pathways and processes. *Nucleic Acids Res.* **37**, D619–D622.
Ma, W., Westmoreland, J. W., Gordenin, D. A. and Resnick, M. A. (2011). Alkylation base damage is converted into repairable double-strand breaks and complex intermediates in G2 cells lacking AP endonuclease. *PLoS Genet.* **7**, e1002059.
Meek, D. W. and Anderson, C. W. (2009). Posttranslational modification of p53: Cooperative integrators of function. *Cold Spring Harb. Perspect. Biol.* **1**, a000950.
Min, K. and Ebeler, S. E. (2008) Flavonoid effects on DNA oxidation at low concentrations relevant to physiological levels. *Food Chem. Toxicol.* **46**, 96–104.
Miyashita, T. and Reed, J. C. (1995). Tumor suppressor p53 is a direct transcriptional activator of the human bax gene. *Cell* **80**, 293–299.
Murray-Zmijewski, F., Slee, E. A. and Lu, X. (2008). A complex barcode underlies the heterogeneous response of p53 to stress. *Nat. Rev. Mol. Cell Biol.* **9**, 702–712.
Neumaier, T., Swenson, J., Pham, C., Polyzos, A., Lo, A. T., Yang, P., Dyball, J., Asaithamby, A., Chen, D. J., Bissell, M. J., *et al.* (2011). Evidence for formation of DNA repair centers and dose-response nonlinearity in human cells. *Proc. Natl Acad. Sci. U.S.A.* **109**, 443–448.
Nikolova, T., Ensminger, M., Löbrich, M. and Kaina, B. (2010). Homologous recombination protects mammalian cells from replication-associated DNA double-strand breaks arising in response to methyl methanesulfonate. *DNA Repair (Amst)* **9**, 1050–1063.
NRC., (2007), *Toxicity Testing in the 21st Century: A Vision and a Strategy*. The National Academies Press, Washington, DC.
Oda, K. and Arakawa, H. (2000). p53AIP1, a potential mediator of p53-dependent apoptosis, and its regulation by Ser-46-phosphorylated p53. *Cell* **102**, 849–862.
Organisation for Economic Co-operation and Development (OECD). (2010). Test No. 487:*In vitro*mammalian cell micronucleus test. *OECD guideline for the testing of chemicals, Section 4*, OECD Publishing, doi:10.1787/20745788.
Paull, T. T., Rogakou, E. P., Yamazaki, V., Kirchgessner, C. U., Gellert, M. and Bonner, W. M. (2000). A critical role for histone H2AX in recruitment of repair factors to nuclear foci after DNA damage. *Curr. Biol.* **10**, 886–895.
Platel, A., Nesslany, F., Gervais, V., Claude, N. and Marzin, D. (2011). Study of oxidative DNA damage in TK6 human lymphoblastoid cells by use of the thymidine kinase gene-mutation assay and the in vitro modified comet assay: Determination of No-Observed-Genotoxic-Effect-Levels. *Mutat. Res.* **726**, 151–159.
Pottenger, L. H., Schisler, M. R., Zhang, F., Bartels, M. J., Fontaine, D. D. and McFadden, L. G. (2009). Dose-response and operational thresholds/NOAELs for in vitro mutagenic effects from DNA-reactive mutagens, MMS and MNU. *Mutat. Res.* **678**, 138–147.
Purvis, J. E., Karhohs, K. W., Mock, C., Batchelor, E., Loewer, A. and Lahav, G. (2012). p53 dynamics control cell fate. *Science* **336**, 1440–1444.
Al Rashid, S. T., Dellaire, G., Cuddihy, A., Jalali, F., Vaid, M., Coackley, C., Folkard, M., Xu, Y., Chen, B. P., Chen, D. J., *et al.* (2005). Evidence for the direct binding of phosphorylated p53 to sites of DNA breaks in vivo. *Cancer Res.* **65**, 10810–10821.
Samanta, S. and Dey, P. (2012). Micronucleus and its applications. *Diagn. Cytopathol.* **40**, 84–90.
Schneider, G., Henrich, A., Greiner, G., Wolf, V., Lovas, A., Wieczorek, M., Wagner, T., Reichardt, S., von Werder, A., Schmid, R. M., *et al.* (2010). Cross talk between stimulated NF-kappaB and the tumor suppressor p53. *Oncogene* **29**, 2795–2806.
Sedelnikova, O. A., Rogakou, E. P., Panyutin, I. G. and Bonner, W. M. (2002). Quantitative detection of (125)IdU-induced DNA double-strand breaks with gamma-H2AX antibody. *Radiat. Res.* **158**, 486–492.
Shieh, S. Y., Ikeda, M., Taya, Y. and Prives, C. (1997). DNA damage-induced phosphorylation of p53 alleviates inhibition by MDM2. *Cell* **91**, 325–334.
Smeenk, L., van Heeringen, S. J., Koeppel, M., Gilbert, B., Janssen-Megens, E., Stunnenberg, H. G. and Lohrum, M. (2011). Role of p53 serine 46 in p53 target gene regulation. *PLoS ONE* **6**, e17574.
Swenberg, J. A., La, D. K., Scheller, N. A. and Wu, K. Y. (1995). Dose-response relationships for carcinogens. *Toxicol. Lett.* **82–83**, 751–756.
Thomas, A. D., Jenkins, G. J., Kaina, B., Bodger, O. G., Tomaszowski, K. H., Lewis, P. D., Doak, S. H. and Johnson, G. E. (2013). Influence of DNA repair on nonlinear dose-responses for mutation. *Toxicol. Sci.* **132**, 87–95.

Thornborrow, E. C., Patel, S., Mastropietro, A. E., Schwartzfarb, E. M. and Manfredi, J. J. (2002). A conserved intronic response element mediates direct p53-dependent transcriptional activation of both the human and murine bax genes. *Oncogene* **21**, 990–999.

Townsend, P. A., Scarabelli, T. M., Davidson, S. M., Knight, R. A., Latchman, D. S. and Stephanou, A. (2004). STAT-1 interacts with p53 to enhance DNA damage-induced apoptosis. *J. Biol. Chem.* **279**, 5811–5820.

Vastrik, I., D'Eustachio, P., Schmidt, E., Gopinath, G., Croft, D., de Bono, B., Gillespie, M., Jassal, B., Lewis, S., Matthews, L., *et al.* (2007). Reactome: A knowledge base of biologic pathways and processes. *Genome Biol.* **8**, R39.

Wyatt, M. D. and Pittman, D. L. (2006). Methylating agents and DNA repair responses: Methylated bases and sources of strand breaks. *Chem. Res. Toxicol.* **19**, 1580–1594.

Xu, Y. (2003). Regulation of p53 responses by post-translational modifications. *Cell Death Differ.* **10**, 400–403.

Yang, L., Allen, B. C. and Thomas, R. S. (2007). BMDExpress: A software tool for the benchmark dose analyses of genomic data. *BMC Genomics.* **8**, 387.

Youlyouz-Marfak, I., Gachard, N., Le Clorennec, C., Najjar, I., Baran-Marszak, F., Reminieras, L., May, E., Bornkamm, G. W., Fagard, R. and Feuillard, J. (2008). Identification of a novel p53-dependent activation pathway of STAT1 by antitumour genotoxic agents. *Cell Death Differ.* **15**, 376–385.

Yu, J. and Zhang, L. (2009). PUMA, a potent killer with or without p53. *Oncogene* **27 (Suppl 1)**, S71–S83.

Zhang, Q., Bhattacharya, S., Andersen, M. E. and Conolly, R. B. (2010). Computational systems biology and dose-response modeling in relation to new directions in toxicity testing. *J. Toxicol. Environ. Health B Crit. Rev.* **13**, 253–276.

Zhao, Y., Katzman, R. B., Delmolino, L. M., Bhat, I., Zhang, Y., Gurumurthy, C. B., Germaniuk-Kurowska, A., Reddi, H. V., Solomon, A., Zeng, M. S., *et al.* (2007). The notch regulator MAML1 interacts with p53 and functions as a coactivator. *J. Biol. Chem.* **282**, 11969–11981.